Marine and Petroleum Geology 132 (2021) 105168

Contents lists available at ScienceDirect

Marine and Petroleum Geology

journal homepage: www.elsevier.com/locate/marpetgeo

Linking facies variations, organic carbon richness and bulk bitumen content – A case study of the organic-rich Middle Triassic shales from eastern Svalbard

Fredrik Wesenlund [a,*], Sten-Andreas Grundvåg [a], Victoria Sjøholt Engelschiøn [b], Olaf Thießen [c], Jon Halvard Pedersen [d]

[a] ARCEx – Research Centre for Arctic Petroleum Exploration, Department of Geosciences, UiT–The Arctic University of Norway, Tromsø, Norway
[b] The Natural History Museum, University of Oslo, Oslo, Norway
[c] Equinor ASA, Harstad, Norway
[d] Lundin Energy Norway, Lysaker, Norway

ARTICLE INFO

Keywords:
eastern Svalbard
Middle Triassic
Botneheia Formation
Facies characterization
Total organic carbon
Bulk bitumen composition
Iatroscan TLC-FID
Multivariate analysis

ABSTRACT

The organic-rich shales of the Middle Triassic Botneheia Formation in Svalbard and its correlative units offshore are considered important source rock intervals for oil and gas generation in the Norwegian Barents Shelf region. Detailed investigation of these intervals is essential to better understand the intra source rock variations and thus to improve exploration models. As source rocks are rarely cored during exploration campaigns, outcrop studies of analogue source rocks onshore Svalbard are of great importance for gaining a comprehensive understanding of the Triassic petroleum system offshore. This integrated sedimentological and geochemical study of the Botneheia Formation investigates the intricate relationship between mudstone facies, total sulfur, total organic/inorganic carbon, and the absolute and relative abundance of bulk bitumen content. Both the Muen Member (Anisian) and the overlying Blanknuten Member (mostly Ladinian) of the Botneheia Formation were densely sampled and analyzed from three outcrop localities on Edgeøya, eastern Svalbard. The results show that total sulfur, total organic carbon, bitumen richness, and relative and absolute aromatic hydrocarbon content increase from bioturbated, gray-colored shales in the lower to middle Muen Member upwards into non-bioturbated, phosphogenic black shales in the middle part of the Blanknuten Member. From here, organic carbon and bulk bitumen richness subsequently decrease upwards in concert with the occurrence of bioturbated, calcareous mudstones and impure limestones towards the top of the Blanknuten Member. Optical vitrinite reflectance variations do not suggest significant maturity variations with depth in the sample profiles, highlighting that the total organic carbon and bulk bitumen content are dominantly coupled with the developing source facies. These facies and chemostratigraphic trends mirror the implied marine vs. terrigenous organic matter sedimentation and benthic preservation potential, which were at a maximum in the middle Blanknuten Member. These processes appear to be closely related to the supply of nutritious upwelled waters that are further linked with an evolving pan-Arctic 2nd order Middle Triassic transgressive–regressive sequence. Facies and multivariate analyses of the geochemical data show that the lower to middle Muen Member are comparable to the pro-delta mudstones of the younger Tschermakfjellet Formation (Carnian), and that both units are clearly distinct from the increased source rock potential and richness in the upper part of the Muen Member and the entire Blanknuten Member. This provides evidence of genetically different paleo-depositional environments and source rock properties that are confined to the lower and upper parts of the Middle Triassic Botneheia Formation, and may have wide applications for Triassic source rock assessment in the offshore Norwegian Barents Sea.

* Corresponding author.
E-mail address: fredrik.wesenlund@uit.no (F. Wesenlund).

https://doi.org/10.1016/j.marpetgeo.2021.105168
Received 21 November 2020; Received in revised form 30 April 2021; Accepted 29 May 2021
Available online 3 June 2021

1. Introduction

The Middle Triassic Botneheia Formation (Fm.) in Svalbard is a regionally extensive, organic-rich 'black' shale deposited during the Anisian–Ladinian (Krajewski, 2008; Leith et al., 1992; Mørk and Bjorøy, 1984) (Fig. 1). The unit is well-exposed across the Svalbard Platform, and thins from c. 150 m thickness in western Spitsbergen to c. 80 m on Edgeøya, further to the east (Mørk et al., 1999). On the Barents Shelf, approximately 550 km south of Svalbard, slightly older, lateral facies-equivalent shale-units are represented by the Olenekian–Anisian Steinkobbe Fm. (Fig. 1c) as documented by shallow bore holes in the Svalis Dome-area (Mørk and Elvebakk, 1999; Vigran et al., 1998) and the 7222/1-1 Aurelia exploration well (Fig. 1a) (Norwegian Petroleum Directorate, 2020). In these two offshore localities (c. 44 km apart), the Steinkobbe Fm. is c. 250 m and c. 280 m thick respectively (Mørk and Elvebakk, 1999; Norwegian Petroleum Directorate, 2020). Collectively, these organic-rich Lower–Middle Triassic formations are considered to host regionally important source rocks extending the Norwegian Barents Shelf.

Basin modelling of the Hammerfest Basin indicates that the Middle Triassic source rocks expelled petroleum as early as c. Early Cretaceous time, with total expelled petroleum estimated to be c. 62 Gt (30 Gt of oil and 32 Gt of gas) (Rodrigues Duran et al., 2013b). Geochemical analyses of petroleum from the Goliat Field support a Triassic source contribution to its Triassic reservoirs (Rodrigues Duran et al., 2013a). Basin modelling further north in the Bjarmeland Platform areas surrounding the Wisting/Hanssen oil discoveries (Fig. 1a) suggests that the Upper Jurassic Hekkingen Fm. is immature, while the Steinkobbe Fm. is early oil expulsion to gas mature in the same area (Stueland, 2016). Source–oil biomarker correlations by Lerch et al. (2018) considered the Olenekian part of the Steinkobbe Fm. as the principal oil contributor to the Wisting/Hanssen oil discoveries. This formation is also indicated to source several other technical oil discoveries (Lerch et al., 2016). The Steinkobbe Fm. and facies equivalents may therefore represent important, oil-prone source rocks that could span more than 250 km in the acreage open to petroleum exploration in the Norwegian Barents Sea. Additionally, the recent report by the Norwegian Petroleum Directorate (2017) estimates that the Middle Triassic source rocks are the most important contributors to liquid petroleum accumulations in the northeastern Norwegian Barents Sea. While this region is not yet open for commercial exploration, it appears that potential Lower–Middle Triassic source rocks may occur throughout large parts of the Norwegian Barents shelf.

Source rock intervals are rarely cored during exploration campaigns, and consequently, there is limited core material available for detailed geochemical analyses of such units. Because Svalbard represents the uplifted and exhumed northwestern corner of the Barents Shelf (Fig. 1a), the Botneheia Fm. may thus serve as a valid facies and geochemical analogue for the under-examined, subsurface Triassic source rock-system offshore. Oil–oil correlation of primary migrated oil (not extract) from an oil-filled ammonoid from the thermally mature Upper Anisian–Ladinian part of the Botneheia Fm. in northwestern Edgeøya (Smelror and Sollid, 2007) suggests a good match with oils from the northwestern Bjarmeland Platform (e. g. 7324/8-1 Wisting Central, 7324/7-2 Hanssen), the Loppa High (e. g. 7220/11-1 Alta, 7222/6-1 S Obesum), the Hammerfest Basin (e. g. 7122/7–3 Goliat - Kobbe & Klappmyss fms.) and the Måsøy Fault Complex (e. g. 7125/4-1 Nucula - Kobbe Fm.) (Thieβen et al., 2019). This justifies the use of the Botneheia Fm. as an analogue for the facies equivalent Steinkobbe Fm.

There are many previous publications that document source rock properties, organic richness and the generation potential of the Botneheia Fm. in Svalbard (e.g. Abay et al., 2017; Abay et al., 2014; Abay et al., 2018; Abdullah, 1999; Bjorøy et al., 2009; Brekke et al., 2014; Forsberg and Bjorøy, 1983; Hubred, 2006; Krajewski, 2008, 2013; Leith et al., 1992; Mørk and Bjorøy, 1984; Riis et al., 2008; Vigran et al., 2008; Xu et al., 2012). In addition, the bulk bitumen content of the Botneheia Fm. shales was recently investigated in detail by Brekke et al. (2014) and Abay et al. (2017). However, few of the previous studies attempt to integrate the stratigraphic distribution of total organic carbon (TOC), total inorganic carbon (TIC), total sulfur (TS) and especially bitumen content in light of the most recent lithostratigraphic subdivision of the Botneheia Fm. by Krajewski (2008). Thus, it appears that a complete understanding of the stratigraphic development of the bulk bitumen content in the Botneheia Fm. is missing.

The majority of previous investigations have focused on the organic-rich paper shales of the mostly Ladinian-aged Blanknuten Member (Mb.) (sensu Mørk et al., 1982). The underlying, Anisian-aged Muen Mb. (sensu Krajewski, 2008) has received notably less attention, probably due to the inferred lower source rock quality and quantity. The bottom conditions during deposition of the shales in the lower to middle part of the Muen Mb. on Edgeøya are debated, and previous studies suggest either dominantly anoxic conditions with absent bioturbation (Vigran et al., 2014), or oxic conditions, with the oxic–sulfidic boundary located primarily below the sediment surface (Krajewski, 2013). The source rock potential of the Muen Mb. might therefore be incorrectly evaluated depending on the chosen depositional interpretation.

The main objective of this study is therefore to characterize chemostratigraphic variations in TOC, TIC, TS and bulk bitumen content (saturates, aromatics and polars) and to tie their relationship to recognized lithostratigraphic changes in the Botneheia Fm. on Edgeøya, eastern Svalbard. Optical vitrinite reflectance data (R_o) of the Muen and Blanknuten mbs. and the Tschermakfjellet Fm. is included to determine the influence of differential thermal maturity variations in the sample profiles. The second objective is to evaluate the depositional conditions of the Muen Mb. and compare it to the overlying Blanknuten Mb. The third objective is to assess the applicability of multivariate exploratory data analysis as a tool to identify genetically different mudstone facies based on the bulk geochemical data. The Blanknuten and Skrukkefjellet localities on northwestern Edgeøya (Fig. 1b) were chosen for this study, as they provide excellent outcrop exposures with minimal structural influence, and because the most recent lithostratigraphic framework is well-established (Krajewski, 2008, 2013).

2. Geological setting

2.1. Tectonostratigraphic development

The end of the Permian resulted in an intracratonic sag basin that covered wide parts of northwestern Pangaea (Faleide et al., 1984, 2015; Glørstad-Clark et al., 2011). This paleo-basin also made up the Triassic Boreal Sea, which was confined by the North American continent towards west, the Panthalassic Sea towards north, Novaya Zemlya towards east, and the northwestern Eurasian plate towards south (Glørstad-Clark et al., 2011) (Fig. 2). During the Early–Middle Triassic, Svalbard received sediments mostly sourced from the west, corresponding to present-day Greenland (Mørk, 2015). A major shift in provenance and sedimentation direction took place in the Late Triassic, when a large deltaic system, which had prograded since Latest Permian from southeast, eventually became the dominating sedimentary system across the entire Barents Shelf (Mørk, 2015). This deltaic system record sediment influx from the development of the Uralian orogeny, ultimately becoming the dominant sediment source of the region (Lundschien et al., 2014) (Fig. 2), and possibly represents the world's largest palaeo-delta system (Klausen et al., 2019). Palynological studies indicate a humid climate regime at the time when the delta-front reached Svalbard in the Late Triassic (Paterson et al., 2017).

In eastern Svalbard, the Middle Triassic Botneheia Fm. is interpreted to represent a 2nd order transgressive–regressive (TR) cycle, possibly reflecting global eustatic sea-level changes over several millions of years due to lithospheric plate movement (Glørstad-Clark et al., 2010; Mørk et al., 1989). Correlative, organic-rich deposits are seen in the Sverdrup Basin, Arctic Canada (Middle Triassic Murray Harbor and Hoyle Bay

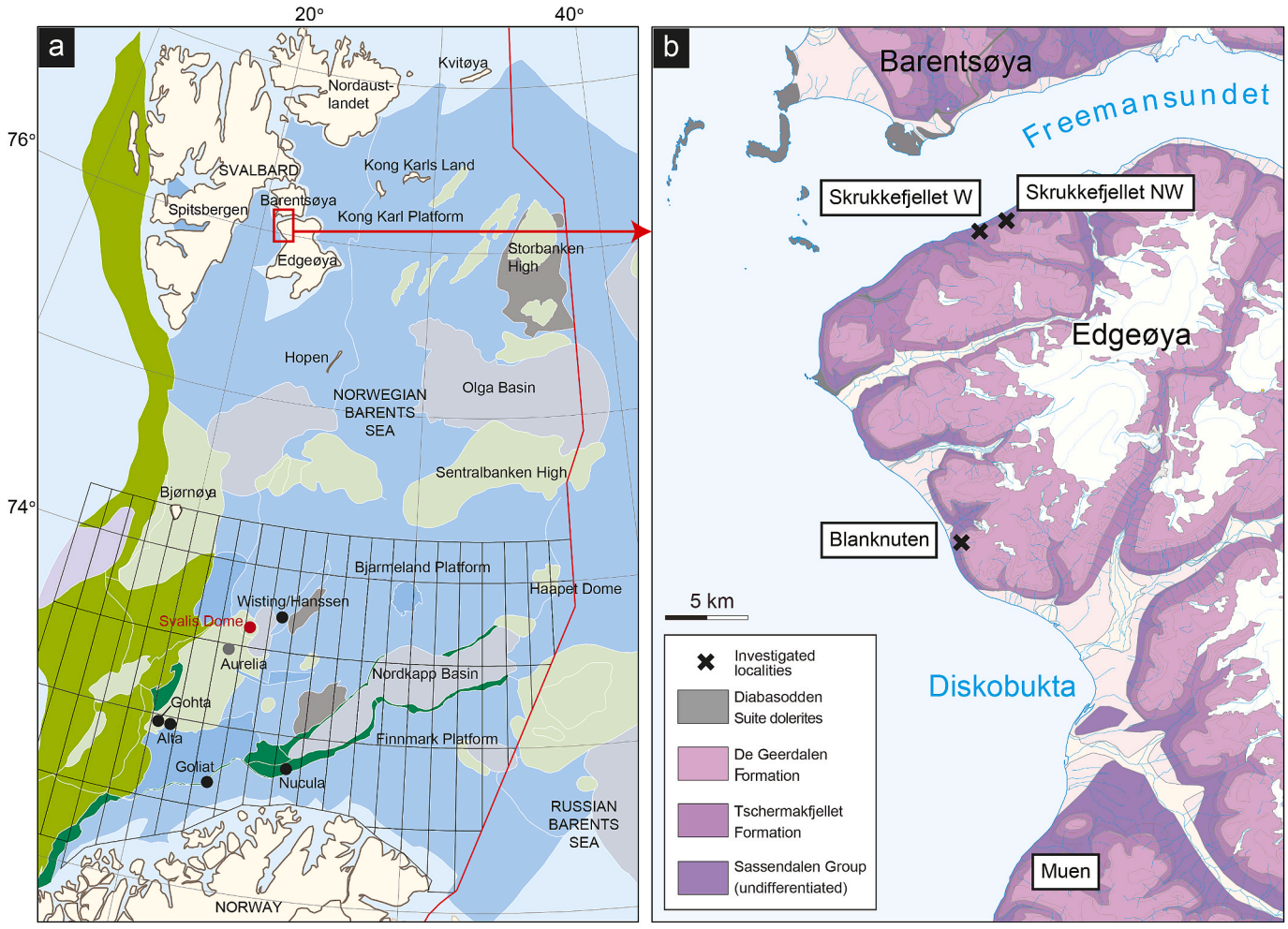

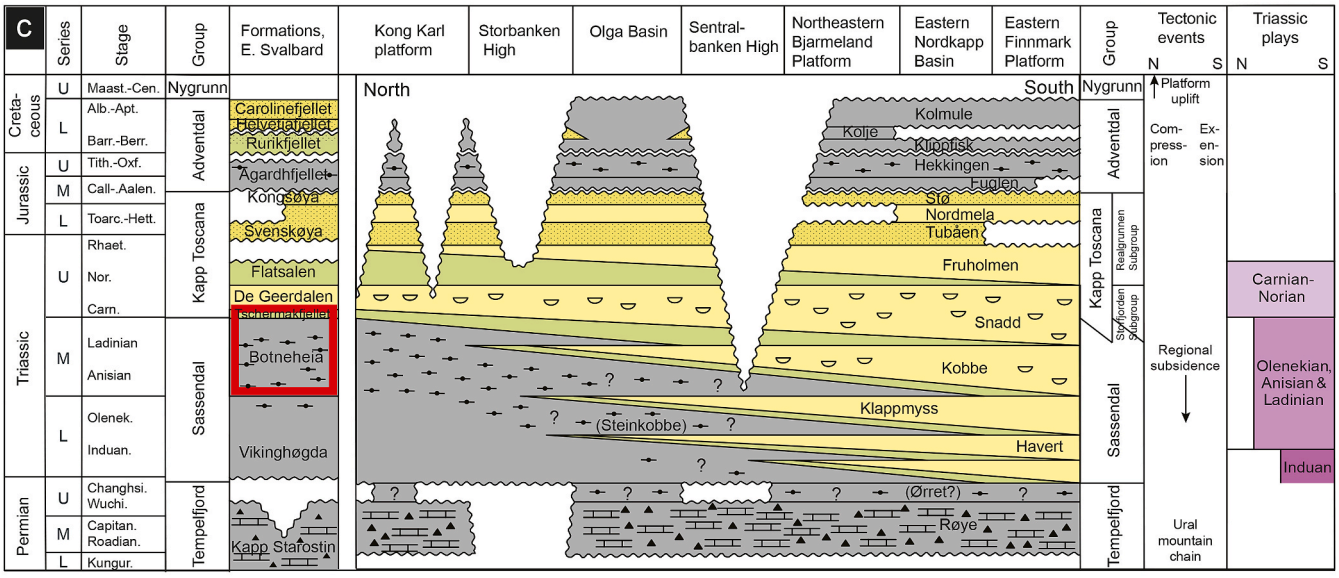

(caption on next page)

Fig. 1. **(a)** Regional map of the Norwegian Barents Sea, where commercially available exploration blocks in areas opened for petroleum activity are shown in the southern part and the area not opened for exploration in the northern part. Modified from the Norwegian Petroleum Directorate (2017). The legend is located below Fig. 1c. **(b)** Local map of the northwestern part of Edgeøya, showing the Blanknuten locality (77°59′43.1″N, 21°11′44.1″E), the Skrukkefjellet W locality (78°09′42.1″N, 21°12′51.1″E), and the Skrukkefjellet NW locality (78°10′10.3"N, 21°18′01.8"E). Modified from Dallmann and Elvevold (2015). **(c)** Chrono- and lithostratigraphic chart of the Permian–Cretaceous periods comparing the offshore Barents Sea to the onshore eastern Svalbard. Note the time-transgressive relationship between the Lower–Middle Triassic Steinkobbe and Middle Triassic Botneheia fms. from south to north. The mapped Triassic plays are included for reference. Modified from the Norwegian Petroleum Directorate (2017).

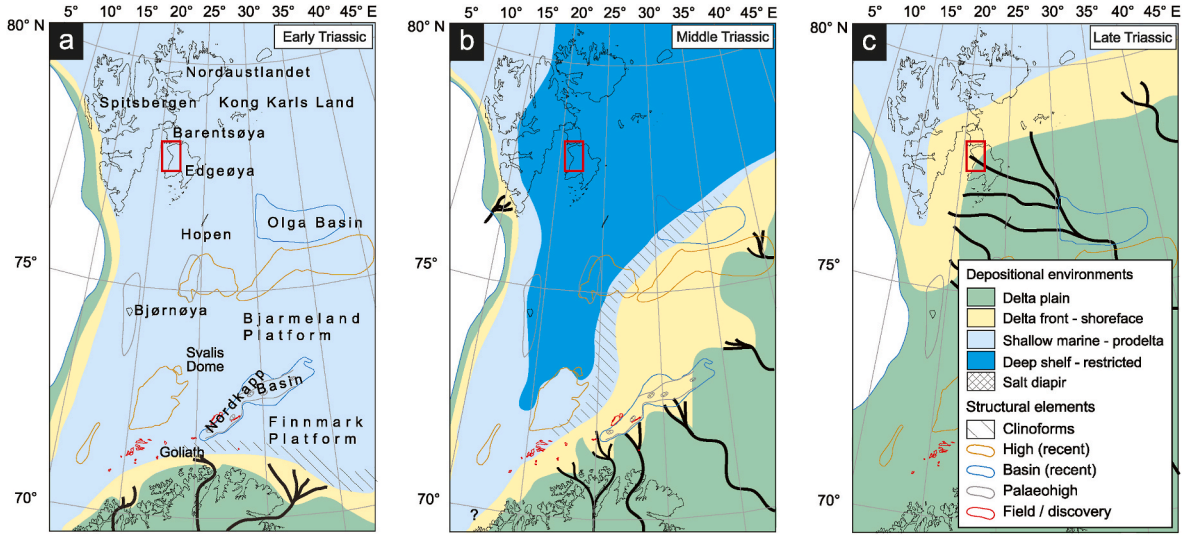

Fig. 2. Early–Late Triassic paleogeography including generalized depositional environments and selected structural elements. The red rectangle marks the study area at Edgeøya. **(a)** Early Triassic. **(b)** Middle Triassic. **(c)** Late Triassic. Modified from Lundschien et al. (2014). (For interpretation of the references to color in this figure legend, the reader is referred to the Web version of this article.)

fms.), and Northern Alaska (Middle–Late Triassic Shublik Fm.) (Leith et al., 1992), as well as in northeastern Greenland in the Wandel Sea Basin (Middle–Late Triassic Israd Fm.) (Alsen et al., 2017; Bjerager et al., 2019). Thus, the Early–Late Triassic Boreal Sea contained widespread organic-rich, fine-grained sediments.

The Triassic period has traditionally been regarded as tectonically quiescent in the northern Barents Shelf (Riis et al., 2008). However, the presence of localized growth faults in the Carnian Tschermakfjellet and De Geerdalen fms. on Edgeøya (Høy and Lundschien, 2011; Smyrak-Sikora et al., 2019) has been linked to a series of deep-rooted normal faults (Anell et al., 2013; Osmundsen et al., 2014). Here, the transition from the shale-dominated Botneheia Fm. to the heterolithic sandstone-bearing Tschermakfjellet Fm. is seen to act as a basal detachment surface for a series of listric faults soling out along the lithological transition (Ogata et al., 2018). Although debated (Klausen, 2013), this could suggest some regional-scale tectonic activity during the Triassic in the northern Barents Shelf (Anell et al., 2013). An angular unconformity between the Upper Triassic and the overlying Lower Jurassic strata in the southern Barents Sea suggests a basin-wide tectonic regime induced by the Novaya Zemlya Fold and Thrust Belt (Muller et al., 2019).

The Barents Shelf records a complex history of differential burial, uplift and erosion through time (Ohm et al., 2008). A regional net erosion estimate of the greater Barents Sea suggest that the southern Barents Shelf was uplifted between 1 and 2 km, increasing monotonically towards northwest, with more than 3 km of uplift and erosion in northwestern Svalbard (Henriksen et al., 2011). However, Marshall et al. (2015) estimate overburden erosion of c. 1.0 km in central Spitsbergen, emphasizing the difficulty of estimating burial depth. In addition, increased magmatic activity during the Early Cretaceous resulted in the High Arctic Large Igneous Province (HALIP) (Ineson et al., 2021; Maher et al., 2004; Senger et al., 2014). In Svalbard, this is manifested by abundant sills and dykes within the sedimentary strata (Mørk and Bjorøy, 1984), often preferentially penetrating the organic-rich Botneheia Fm. (Hubred, 2006). The burial, uplift and erosion coupled with igneous intrusions provide a complex thermal maturation pattern throughout eastern Svalbard, ranging from immature to overmature (Haile et al., 2018).

In the Muen locality on Edgeøya (Fig. 1b), the Botneheia Fm. is late mature, but no igneous intrusions are outcropping (Brekke et al., 2014; Mørk and Bjorøy, 1984). This could indicate the presence of a subsurface igneous body with a sufficient thickness that have thermally affected the Botneheia Fm. in this locality (Brekke et al., 2014; Hubred, 2006; Mørk and Bjorøy, 1984). 20 km northwards in the Blanknuten locality (Fig. 1b), the Botneheia Fm. shows T_{max} ranging from 440 to 447 (°C) (Krajewski, 2013), suggesting a thermally mature outcrop section. This maturation is dominantly caused by progressive burial (Haile et al., 2018), indicating that sills or dykes have insignificant thermal contribution and that the inferred underlying igneous body in the south probably does not affect the Botneheia Fm. this far north. This can also be assumed for mudstones from the Skrukkefjellet locality (Fig. 1b) on northern Edgeøya as they are less mature than those from the Blanknuten locality (Mørk and Bjorøy, 1984; Schou et al., 1984). T_{max} data from the Skarpryttaren locality c. 10 km north of the Skrukkefjellet locality range from 435 to 443 (°C) (Krajewski, 2013), confirming a northwards decreasing maturity trend from the Blanknuten locality.

2.2. *Lithostratigraphic framework and sedimentology of the Middle Triassic, Eastern Svalbard*

The Botneheia Fm. is considered to conformably overlie the Olenekian-aged Vendomdalen Mb. of the Lower Triassic Vikinghøgda Fm. (Brekke et al., 2014; Høy and Lundschien, 2011), although this boundary might also represent a disconformity (Hounslow et al., 2008). In eastern Svalbard, Krajewski (2008) subdivided the Botneheia Fm. into nine informal units based on litho- and chemostratigraphic

characteristics (unit 1 to unit 9). Lithostratigraphically, units 1 to 5 represent the Muen Mb., and units 6 to 9 represent the Blanknuten Mb. In addition, Krajewski (2008) identified two dominant chemostratigraphic units consisting of a lower non-phosphogenic (corresponding to units 1–4) and an upper phosphogenic facies (corresponding to units 5–9). Note that these two chemostratigraphic units do not correspond directly to the formal lithostratigraphic member division.

On Edgeøya, the boundary between the Botneheia Fm. and the overlying Tschermakfjellet Fm. is rather sharp and abrupt (Fig. 3a), suggesting that it might represent a break in deposition or a submarine hiatus developing at the Ladinian–Carnian boundary (Mørk et al., 1989). The Tschermakfjellet Fm. consists of mainly dark gray mudstones (Fig. 3g) enriched in terrestrial organic matter (Mørk and Bjorøy, 1984). In the northern Barents Sea, the Tschermakfjellet Fm. is seen to downlap (in a continuous fashion) onto the top surface of the Botneheia Fm., suggesting a pro-delta (bottomset) origin for these early Carnian deposits (Høy and Lundschien, 2011). A pro-delta origin is supported by its stratigraphic position below the transitionally overlying fluvio-deltaic De Geerdalen Fm., which prograded from the southeast during Carnian times (Lord et al., 2017). *Tasmanites* algae have been recorded in the lowermost part of the Tschermakfjellet Fm. (Vigran et al., 2014).

In the present study, we refer to units 1 to 4 of Krajewski (2008) collectively as the *lower–middle Muen Mb.*, unit 5 as the *upper Muen Mb.*, unit 6 and unit 7 as the *lower* and *middle Blanknuten mbs.*, respectively, and the combined units 8 and 9 as the *upper Blanknuten Mb.* (Table 1).

The non-phosphogenic lower–middle Muen Mb. (Anisian, unit 1 to unit 4; Table 1) consists mostly of gray to dark-gray mudstones and occasional centimeter–decimeter-scale carbonate and siltstone beds (Fig. 3a and b) (Krajewski, 2008), also shown in this study (section 4.1). Although Vigran et al. (2014) and this study report *in situ* phosphate nodules at this stratigraphic level in the studied localities, we apply the term non-phosphogenic as the mudstone matrix from this succession is dominantly phosphate-free (Krajewski, 2008). The upper part (i.e. unit 5) contains black shales (Fig. 3c) with common occurrences of macroscopic phosphate nodules. Krajewski (2008) attributes the non-phosphogenic part of the Muen Mb. (units 1 to 4) to represent deposition under mainly oxic conditions with moderate primary productivity and increased terrestrial runoff, ultimately resulting in varying source rock quality (median HI = 281 ± 52 mg HC/g TOC, 1σ) and richness (median TOC = 2.63 ± 1.08 wt. %, 1σ) (Krajewski, 2013). In contrast, the upper phosphogenic part of the Muen Mb. (unit 5) is interpreted to represent the onset of periods with increased primary productivity, as indicated by the presence of black shale containing pristine, macroscopic phosphate nodules. This chemostratigraphic transition suggest a change from an oxic, early transgressive phase to an oxic–dysoxic, late transgressive phase (Krajewski, 2008).

The overlying, phosphogenic facies-dominated Blanknuten Mb. (mainly Ladinian, unit 6 to unit 9) forms a characteristic black cliff along the coastline of Edgeøya (Fig. 3a). It consists of dominantly black-colored, calcareous, organic-rich mudstones with calcareous siltstone beds and silty limestone beds (Mørk et al., 1982, 1999). These shales contain dominantly kerogen type II, with TOC values ranging from c. 2–11 wt. % (Krajewski, 2013).

The lower part of the Blanknuten Mb. (unit 6 of Krajewski, 2008, Table 1) consists of mostly black, laminated shale with abundant pristine and macroscopic phosphate nodules (Fig. 3d), suggesting deposition under high primary productivity in dysoxic to anoxic conditions (Krajewski, 2013). The middle part of the member (i.e. unit 7 of Krajewski, 2008, Table 1) consists of massive, cliff-forming, paper-laminated shale (Fig. 3e), which marks increased stagnation with subsequent regional anoxia. On northwestern Edgeøya and southern Barentsøya (Fig. 1b), this unit has excellent richness (median TOC = 8.10 ± 1.06 wt. %, 1σ) and oil generation potential (median HI = 538 ± 42 mg HC/g TOC, 1σ), and is considered the best source rock unit within the Botneheia Fm., presumably deposited during a Middle Triassic eustatic sea-level high-stand phase (Krajewski, 2013). A maximum flooding surface is located in the lower part of unit 7 (Krajewski, 2013), which occurred during early Ladinian (Krajewski and Weitschat, 2015). The upper part of the member (units 8 and 9 of Krajewski, 2008, Table 1) consists mainly of fissile mudstones (Fig. 3f) with abundant reworked phosphate nodules and phosphate-filled flattened *Thalassinoides* burrows (Mørk and Bromley, 2008). Siltstone interbeds (interpreted as distal storm deposits) are common, contrasting the underlying massive, cliff-forming shale (Mørk and Bromley, 2008). The facies variability indicates recurrent changes in the benthic environment triggered by a regressive trend with fluctuating oxic to anoxic conditions (Krajewski, 2013; Mørk and Bromley, 2008).

3. Samples and methods

3.1. Field work

A complete vertical section of the Botneheia Fm. (and the lowermost few meters of the overlying Tschermakfjellet Fm.) was logged for sedimentary features and concertedly sampled in the Blanknuten locality (Bernhardsen, 2019). Two stratigraphically incomplete, but partly overlapping sections were sampled at Skrukkefjellet W (exposing the lower part of the formation) and Skrukkefjellet NW (exposing the upper part of the formation; Fig. 1b). These are combined to form a stratigraphically complete, composite sample profile of the Botneheia Fm. at Skrukkefjellet. Although the two sections at Skrukkefjellet are located c. 2 km apart (Fig. 1b for location), the excellent outcrop quality makes physical and visual tracing of the main stratigraphic units possible, ensuring that the composite sample profile represents a complete section through the formation. For all sections, sample pits were dug (average sample interval: < 2 m) in the slope or outcrop whenever possible, and *in situ* rock material was collected to minimize weathering influence and contamination from recent organic matter. Although siltstone/cementstone beds and concretions were partly sampled along-side mudstones, this study pertains to the latter.

3.2. Sample preparation

Prior to geochemical analysis, the outcrop samples were rinsed and scrubbed in temperate, running water. Rock material with weathering skins, contemporary organic matter or abundant calcite veins was discarded. The samples were dried at < 30 °C overnight. Macroscopic phosphate nodules were removed to obtain comparable samples of mudstone matrix composition. Still, abundant phosphate content cannot be ruled out. The samples were crushed to gravel size using an agate mortar and pestle. 1 dl of the crushed sample material was milled using a Retsch PM 100 with agate chamber and agate milling balls set at 450 rpm for 10 min, resulting in a homogenized, fine rock powder.

3.3. LECO combustion

101 samples were quantified for TS, TOC and total carbon (TC) using a LECO™ CS744 carbon/sulfur determinator (Table 1). Prior to analysis, 2.0 g of the pulverized sample material was dried at 105 °C overnight. For TS and TC analysis, between 0.23 and 0.25 g of the dry, heated sample was weighed in a single-use crucible. For TOC analysis, between 0.40 and 0.45 g of dry heated sample was weighed in a single-use fluid-permeable crucible, and subsequently acid treated with 10% HCl and rinsed with water until no reaction between the acid and powder was observed. The acid treated samples were dried at 105 °C overnight. The TOC and TC/TS prepared samples were combusted with accelerators to facilitate combustion, with an instrument run time set at 70 s. TIC was calculated by subtracting TOC from TC.

3.4. Bitumen extraction

Based on the LECO analysis, 57 samples (Table 1) were picked for

Fig. 3. Lithostratigraphic boundaries and facies of the Botneheia Fm. in the Blanknuten locality. **(a)** Overview of the Muen and Blanknuten mbs. Stratigraphic boundaries (dashed lines), phosphogenic facies, and kerogen types adapted from Krajewski (2008, 2013). Note that the entire Blanknuten Mb. is phosphogenic. **(b)** Dark gray, flaky, non-phosphogenic mudstone (F1), lower–middle Muen Mb. **(c)** Flaky to platy, black mudstone (F2) from phosphogenic upper Muen Mb. **(d)** Massive, black, platy mudstone (F2) with defined fissility of the lower Blanknuten Mb. White arrows indicate abundant phosphate nodules. **(e)** Outcrop expression of the fissile mudstone (F3) of the massive middle Blanknuten Mb., yielding platy fragments. Gray weathering skin masks the true black color of the mudstone. **(f)** Platy, highly fissile outcrop expression of the black mudstones (F4) in the upper Blanknuten Mb. Arrows denote flattened phosphate-precipitated burrows. **(g)** Flaky fragmentation and crumbled outcrop expression of the dark gray mudstones (F1) in the lowermost Tschermakfjellet Fm. The marker pen in panels b–e measures 14 cm. Locations are given in Fig. 1b. (For interpretation of the references to color in this figure legend, the reader is referred to the Web version of this article.)

Table 1
Comparison between the amount of analyzed samples and coinciding stratigraphic units from Krajewski (2008) and this study.

Stratigraphic unit, this study	Stratigraphic unit, Krajewski (2008)	Samples analyzed	
		LECO	Iatroscan TLC-FID
lower–middle Muen Mb.	Units 1–4	32	12
upper Muen Mb.	Unit 5	6	4
lower Blanknuten Mb.	Unit 6	15	11
middle Blanknuten Mb.	Unit 7	30	19
upper Blanknuten Mb.	Units 8–9	15	8
Tschermakfjellet Fm.	Tschermakfjellet Fm.	3	3

bitumen extraction using a ST 243 Soxtec™ system. Empty cellulose extraction thimbles were boiled for 10 min and rinsed for 20 min using 100 ml of DCM:MeOH (93:7 vol. %) solvent prior to sample extraction to remove possible contaminants. c. 10 g of powdered sample material was inserted into the pre-extracted thimbles. Elemental copper beads were added to the extraction cups as boiling stones and to remove residual sulfur. The samples were boiled for 60 min and rinsed for 120 min with 100 ml of solvent, later concentrated to 0.5 ml by solvent evaporation in a fume hood. The concentrated extracts were not deasphaltened.

3.5. Iatroscan TLC-FID

An Iatroscan™ MK-5 thin layer chromatography – flame ionization detector (TLC-FID) was used to separate and quantify the absolute and normalized (% by weight) saturate (SAT), aromatic (ARO) and polar (POL; resins + asphaltenes) fractions of the total bitumen extracts (Karlsen and Larter, 1991). 3 μl or 2 μl depending on extract richness of 3.85 vol. % strength of the 0.5 ml extract concentrate was applied onto silica gel-coated rods (type Chromarod IV). Variations in analyte volume were necessary to prevent column overload and subsequent poor peak separation. The silica rods were lowered into containers of cyclohexane for 20 min and toluene for 8 min to elute and separate the SAT and ARO fractions respectively. The POL fraction remained stationary and was thus also separated from the other fractions. The applied rods were dried for 2 min in between each elution and ultimately dried at 40 °C for 40 s to remove solvents prior to analysis. Scan time was set to 30 s, with H_2 and O_2 flow set at 180 ml/min and 2.1 l/min respectively. A blank sample and the Norwegian Geochemical Standard NSO-1 (Weiss et al., 2000) were used for quality checking each run. Analytical precision was 46.5 ± 1.0%, 25.0 ± 1.0%, and 28.6 ± 2.0% (n = 4, 1σ) for the normalized (by weight) SAT, ARO and POL fractions of non-deasphaltened NSO-1 respectively. This yielded a mean SAT/ARO ratio of 1.86 ± 0.03 (1σ), i.e. within the permissible range of c. 1.3–2.0 (Weiss et al., 2000). Response factors for the SAT, ARO and POL fractions were 0.000607249, 0.000564736 and 0.000328987 respectively. The SES-i-ChromStar software were used to analyze and quantify the bitumen fractions by peak area integration of manually interpreted base lines. The absolute extractable organic matter (EOM) was back calculated to original concentration (100% vol. strength) and is reported in mg/g rock.

3.6. Vitrinite reflectance

The vitrinite reflectance analysis was carried out by Applied Petroleum Technology (APT) in Norway. They applied the following methods: The kerogen was isolated using standard palynological procedures, i.e. HCl and HF treatment followed by floating in $ZnBr_2$, subsequently agitated with ultrasonic energy and then centrifuged. A +10 μm fraction of the sieved and floated kerogen was mounted with resin on petrographic slides and polished with water. Reflectance measurements were made with a Zeiss™ Epiplan – Neofluar 40X oil immersion objective in light at a wavelength of 546 nm (green). The measurements were random (R_o) in nominally unpolarized light. Vitrinite phytoclasts were searched for until 55 have been measured or for half an hour, whichever was the sooner. The sample quality was considered good, i.e. the vitrinite type, quality, size or abundance had no effect on the readings.

3.7. Exploratory data analysis

The exploratory data analysis includes principal component analysis (PCA) and hierarchical cluster analysis (HCA), two common techniques for investigating depositional environment, maturity and correlations of source rocks and crude oils (Peters et al., 2005, 2007; Wang et al., 2018). All samples subjected to both LECO and Iatroscan analysis were included, amounting to a 57 samples (rows) by 13 variables (columns) data matrix. Each column of the matrix was scaled to a range of [0, 1] using min–max feature scaling. The analysis was performed using Python (v. 3.8.5) coupled with the sklearn (v. 0.23.2) and seaborn (v. 0.11.0) software libraries for PCA and HCA respectively. The Python script is open access (see section 7). For the HCA, the distance metric was set to "euclidean", while the linkage method was set to "average", which apply the unweighted pair group method with arithmetic mean algorithm (UPGMA). The color palette for the stratigraphic units is from Wong (2011).

4. Results

4.1. Stratigraphic units and boundaries

At the Blanknuten locality, all internal lithostratigraphic boundaries of the Botneheia Fm. are easily recognized by contrasting outcrop weathering expressions (Fig. 3a–f), except the boundary from the lower–middle Muen Mb. to the upper Muen Mb. The base Muen Mb. boundary, i.e. the base Botneheia Fm., lies immediately above slightly darker mudstones of the Vikinghøgda Fm. (Fig. 3a). The bulk Muen Mb. displays an upwards increase in dm-scale event beds, useful to distinguish the lower–middle Muen Mb. and the upper Muen Mb. (Fig. 3a). However, the lower–middle to upper Muen Mb. boundary is inferred based on contrasting facies (see section 4.2 for facies description). Also within the Blanknuten Mb., each sub-unit is visually discernible (Fig. 3d–f), as is the transition into the Tschermakfjellet Fm., marking an abrupt change in the weathering expression and shale fragment morphology (Fig. 3a and g). At this locality, the Botneheia Fm. was measured to be c. 75 m thick.

At the Skrukkefjellet W locality (Fig. 4a), it was difficult to determine the boundary between the upper Muen Mb. and the lower Blanknuten Mb., as the slope morphology changes with varying slope gradients. In addition, two normal faults (related to outcrop failure) were recognized within the apparent monotonous shale succession (Fig. 4a). Displacement in the Muen Mb. (corresponding to units 1 to 5 of Krajewski, 2008, Table 1) and the lower Blanknuten Mb. (unit 6 of Krajewski, 2008, Table 1) is in the order of several meters. The boundaries between the Muen Mb. and the overlying lower Blanknuten Mb., as well as between the lower and middle parts of the Blanknuten Mb. appear to be juxtaposed (Fig. 4a). The southern fault is clearly recognized in map view as a south-dipping normal fault with E–W apparent strike (Fig. 4b). Thus, if not carefully considered, logging the section from south to north on the topographic ridge (which is the most natural thing to do) will inevitably result in several meters of repeated strata, and consequently an overestimated formation thickness.

A tub-like discoidal concretion has previously been reported from the Skrukkefjellet W locality (Vigran et al., 2014, their Fig. 49b). This feature is easily recognized and provides an excellent reference point in the outcrop (Fig. 4a, c, d) and map view (Fig. 4b). Based on our field observations and correlation to previous studies (Krajewski, 2008, 2013; Vigran et al., 2014), the base Blanknuten Mb. boundary is placed at the base of this characteristic discoidal concretion. This horizon appears to host several other concretions in the Skrukkefjellet Mountain. The base

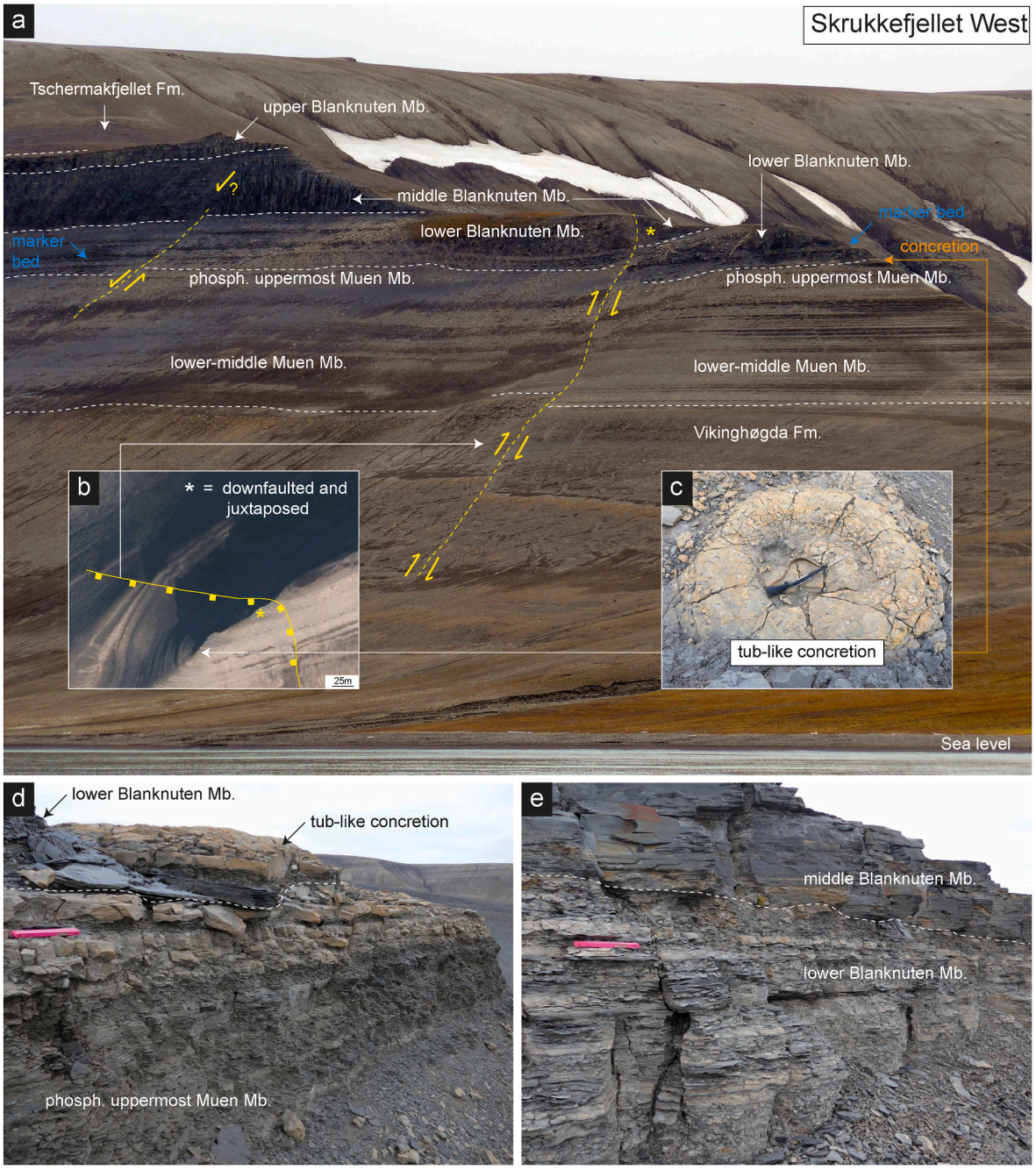

Fig. 4. Overview of the Botneheia Fm. in the Skrukkefjellet W locality with annotated lithostratigraphic and structural boundaries and features. **(a)** Overview photograph with stratigraphic boundaries (white dashed lines) and normal fault planes (dashed yellow lines). Juxtaposition of the lower Blanknuten Mb. and middle Blanknuten Mb. in the footwall is shown in the upper right of the picture, marked with a yellow asterisk (*). The marker bed (blue arrow) potentially marks the correct Blanknuten Mb. lower boundary. **(b)** Map view of the fault plane, roughly indicating an E–W strike with southerly dip. The yellow asterisk (*) marks the same downfaulted part as in panel a. Map retrieved from the Norwegian Polar Institute (2020). **(c)** A characteristic, discoidal tub-like concretion seen at the southern ridge in the locality. The orange and white arrows mark the concretion in panels a and b respectively. Ruger M77 Hawkeye rifle (c. 110 cm) for scale. **(d)** Close-up of the phosphogenic upper Muen Mb. (F2), showing the member boundary just underneath the tub-like concretion. The pink ruler is c. 23 cm. **(e)** outcrop expression of the lower–middle Blanknuten Mb. boundary, showing the characteristic change from dark gray to black mudstones (F2) to black calcite cemented, massive and smooth shales (F3). Pink ruler is c. 23 cm. Locations are given in Fig. 1b. (For interpretation of the references to color in this figure legend, the reader is referred to the Web version of this article.)

of the middle Blanknuten Mb. boundary is arguably the most recognizable sub-unit boundary within the Botneheia Fm. as it marks an abrupt transition from nodule-rich to nodule-free mudstones (Fig. 4e). In contrast, the boundary between the middle to uppermost Muen Mb. was not pinpointed in the field but is inferred based on facies variations (see section 4.2 for facies descriptions).

Owing to the faulted strata in the Skrukkefjellet W locality, the top lower Blanknuten Mb. and the entire middle and upper Blanknuten Mb. and the lowermost Tschermakfjellet Fm. were sampled at the Skrukkefjellet NW locality (Fig. 5). While all the main stratigraphic units may be recognized at the Skrukkefjellet NW locality, scree hindered detailed observations of the entire Muen Mb. and the lower Blanknuten Mb. (Fig. 5a and b). Intra-Blanknuten Mb. stratigraphic boundaries are easily recognized (Fig. 5c and d). The lower–middle Blanknuten Mb. boundary

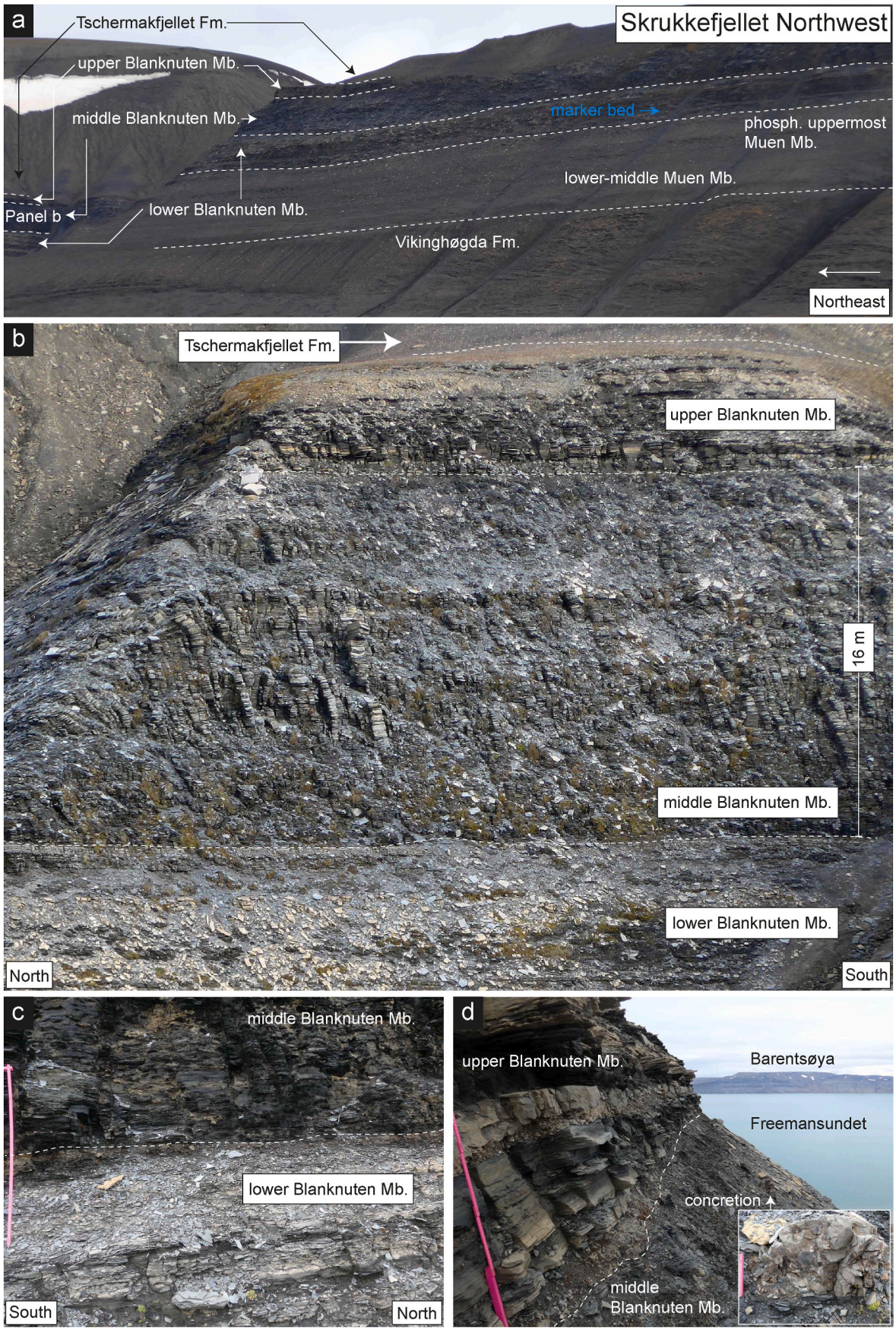

(caption on next page)

Fig. 5. Outcrop expression of the Botneheia Fm. in the Skrukkefjellet NW locality with annotated stratigraphic units and boundaries. **(a)** Overview photograph with stratigraphic boundaries. Here, the bulk Muen Mb. and much of the lower Blanknuten Mb. is covered by scree. No faulting is observed. The marker bed in blue possibly indicates the base Blanknuten Mb., see section 5.1 for discussion. **(b)** Overview photograph showing the weathering expression of the lower Blanknuten Mb. upwards into the Tschermakfjellet Fm. The middle Blanknuten Mb. shows characteristic weathering-formed columnar stacks of F3 mudstones. Note that this photograph represents the eastern side (78°10′08.9″N, 21°18′57.6"E) of an N–S trending unnamed valley in the Skrukkefjellet NW locality. The samples from this locality were collected c. 350 m directly west from this cliff face (78°10′10.3"N, 21°18′01.8"E). **(c)** Close-up of the lower–middle Blanknuten Mb. boundary (dashed line), displaying a sharp color contrast between these units. Pink ruler measures 1 m. **(d)** Close-up of the middle–upper Blanknuten Mb. boundary (dashed line), looking N–NW towards Barentsøya. The base is defined by the change from fissile shales (F3) below and the occurrence of yellowish gray siltstone/cementstone interbedding the F4 mudstones. Pink ruler measures c. 65 cm in the photograph. Locations are given in Fig. 1b. (For interpretation of the references to color in this figure legend, the reader is referred to the Web version of this article.)

marks the transition from brighter, weathered rock fragments, sharply changing into black, fissile, cliff-forming shales making up the base of the Blanknuten Mb. cliff in this locality (Fig. 5c). The boundary between the middle and upper parts of the Blanknuten Mb. is characterized by a change from cemented and massive, fissile mudstones into more yellowish fissile mudstones with abundant macroscopic phosphate nodules and interbeds of cemented siltstones (Fig. 5d).

A laterally extensive carbonate-cemented siltstone bed forms the base of dense, cliff-forming, black mudstones in the coastal exposures of Skrukkefjellet (highlighted with blue text and arrow; Figs. 4a, 5a and 6a, 6b). The significance of this bed is discussed in Section 5.2. Selected features from the Blanknuten Mb. are included in Fig. 7 and will be tied to the facies description below.

4.2. Facies description

The facies division presented here is based on distinct visual and textural differences observed in various mudstone types seen in the

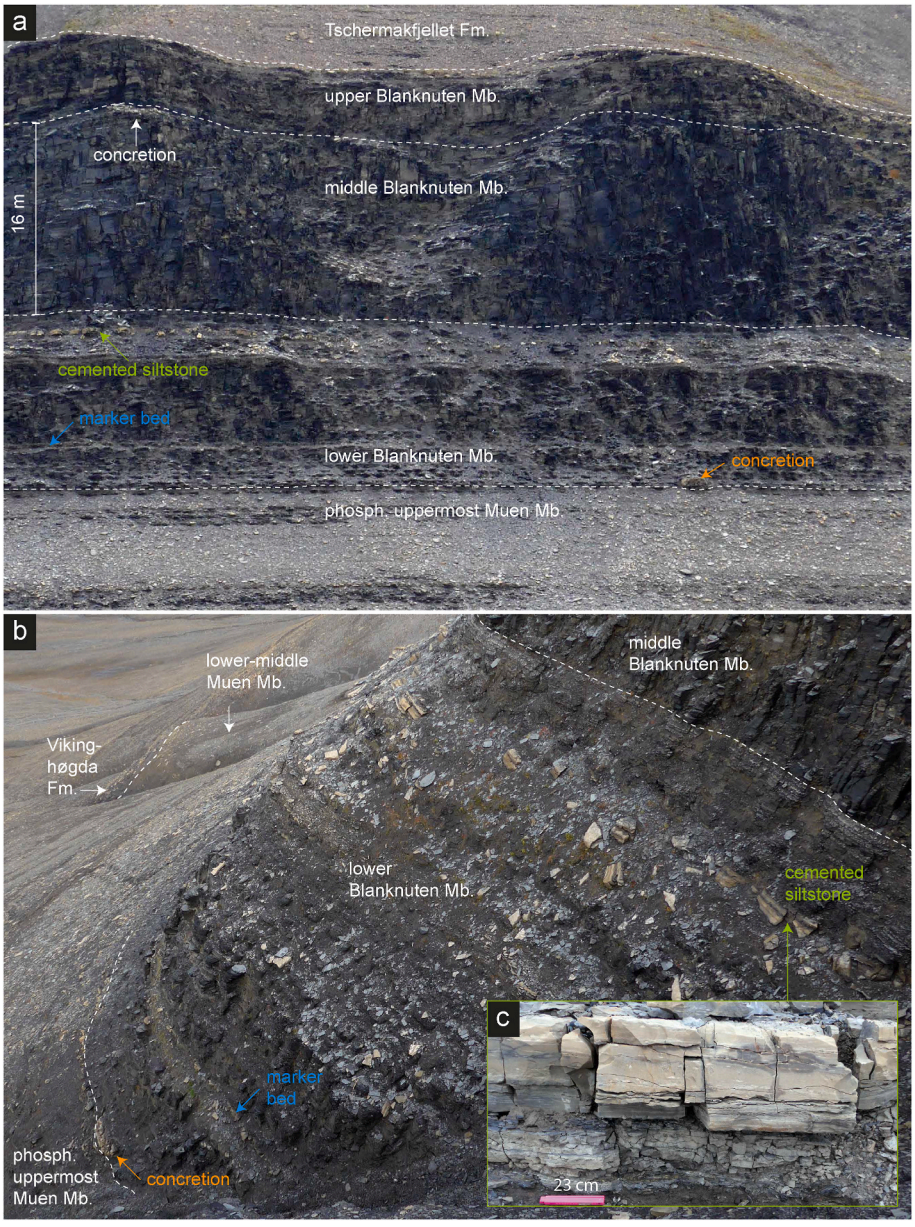

Fig. 6. Outcrop expression of the Blanknuten Mb. in the north face of the Skrukkefjellet Mountain. **(a)** Lithostratigraphic division, highlighting a concretion (orange arrow) at the same stratigraphic level as the concretion shown in Fig. 4c. A continuous marker bed (blue arrow) marks the onset of cliff-forming black shales in certain gentler-sloping areas of Skrukkefjellet. The upper concretion (white arrow) marks the uppermost part of the middle Blanknuten Mb. and is c. at the same stratigraphic level as the concretion in Fig. 5d. A c. 0.5 m siltstone bed (green arrow) is highlighted for reference. **(b)** Overview of the lower Blanknuten Mb., showing its lower cliff-forming part (F2), and the more scree covered upper part. The colored arrows refer to equivalent beds and concretion at the same stratigraphic height as explained in panel a. The thickness of the lower Blanknuten Mb. is c. 16 m. **(c)** A continuous carbonate cemented siltstone bed, acting as a marker in the upper part of the lower Blanknuten Mb. Folded meter stick (23 cm) for scale. (For interpretation of the references to color in this figure legend, the reader is referred to the Web version of this article.)

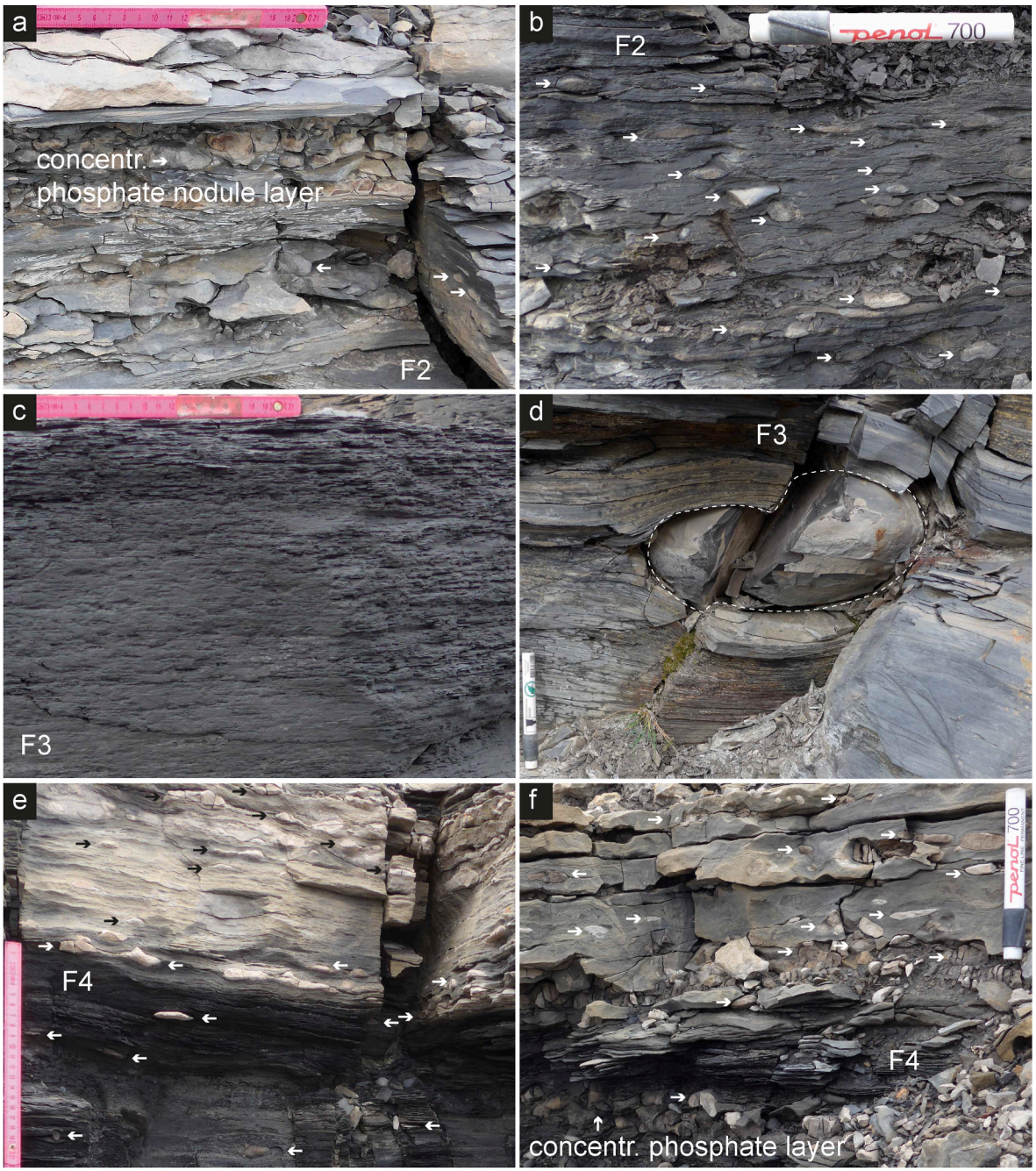

Fig. 7. Outcrop expression of identified facies in the Blanknuten Mb. **(a)** Phosphate grainstone beds and interbeds of phosphatic mudstones (F2) containing phosphate nodules. lower Blanknuten Mb., Skrukkefjellet W. **(b)** Massive, black mudstones (F2) with abundant phosphate nodules. lower Blanknuten Mb., Blanknuten type locality. **(c)** Massive and fissile black shales (F3) with no apparent bioturbation. middle Blanknuten Mb., Skrukkefjellet W. **(d)** Massive, fissile shales (F3) with a dark gray, authigenic calcite concretion. Note the deformed shales around the concretion. middle Blanknuten Mb., Blanknuten. **(e)** Black and yellow weathering fissile mudstones (F4) with ovoidal to irregular authigenic phosphate nodules. upper Blanknuten Mb., Skrukkefjellet NW **(f)** Cemented siltstone bed with reworked phosphate nodules, interbedded with mudstones (F4). upper Blanknuten Mb., Skrukkefjellet NW. Arrows denote phosphate nodules. Locations are given in Fig. 1. (For interpretation of the references to color in this figure legend, the reader is referred to the Web version of this article.)

Muen and Blanknuten members, and Tschermakfjellet Fm. (Fig. 8). This method is commonly applied in the description of core cuttings during well-site operations (Whittaker and Morton-Thompson, 1992). A brief description of the four types of visually discernible mudstone facies is provided below. Note that the mudstone facies recognized in this study partly correspond to those of Krajewski (2008).

Facies 1 (F1). This facies (Fig. 8a) occurs in the lower and middle parts of the Muen Mb. (Fig. 3b). and in the lowermost Tschermakfjellet Fm. (Fig. 3g). It consists of gray to dark gray mudstone and shows variable fissility. Fragmentation is both concoidal and platy, but is generally seen to yield flaky fragments, commonly associated with non-laminated fabric. The bedding surface of fragments lacking fissility may be rough, depending on degree of bioturbation. Cleavage surfaces do not necessarily follow bedding surfaces. Bioturbation in both localities is mainly seen as scattered, gently curved, mm-scale burrows (Fig. 8b). The burrows are darker than the mudstone matrix, possibly due to pyritization. Two samples

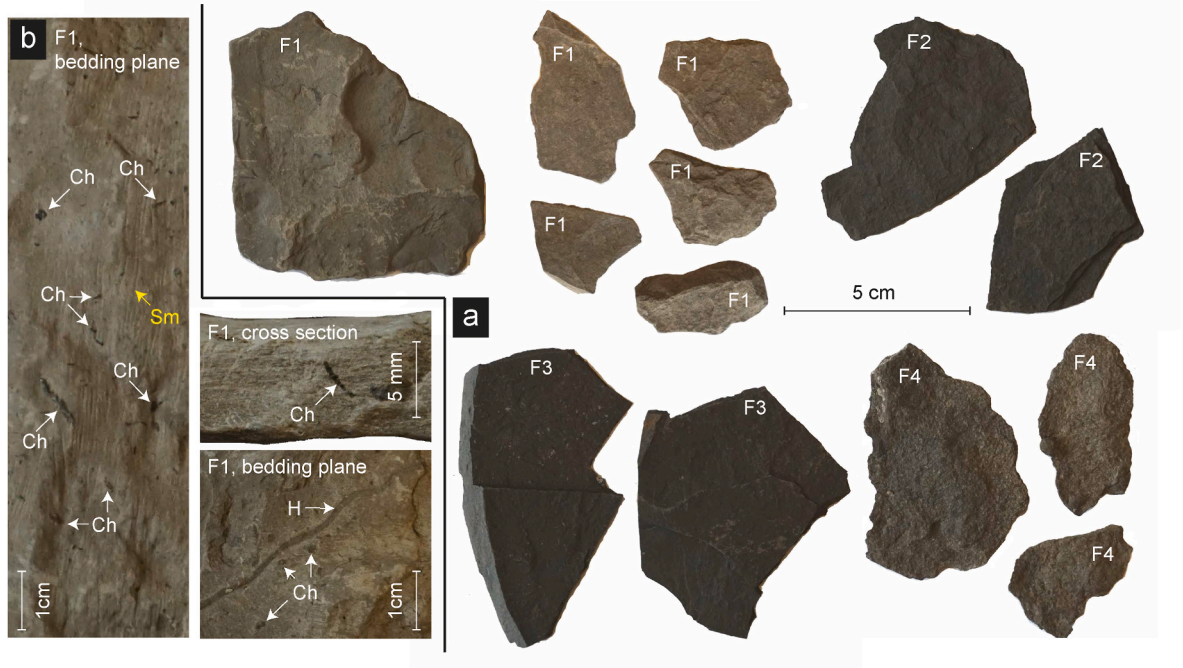

Fig. 8. **(a)** Images of dried shale fragments of facies F1–F4 shot at constant ISO, aperture, shutter speed and white balance settings, allowing for direct comparison of color and brightness. The large F1 fragment represents the lower–middle Muen Mb., while the smaller F1 fragments represents the Tschermakfjellet Fm. The F2, F3 and F4 fragments represent the upper Muen Mb., middle Blanknuten Mb., and upper Blanknuten Mb. respectively. **(b)** Images of F1 mudstone with traces of interpreted *Chondrites* (Ch) and *Helminthopsis* (H), see sections 4.1 for description and 5.2 for interpretation. Scratch marks (Sm) are recent and not related to geological processes. (For interpretation of the references to color in this figure legend, the reader is referred to the Web version of this article.)

at levels 28 and 30 m in the Skrukkefjellet W section show unbranched, mm wide, cylindrical and smooth horizontal trails with winding pattern (Fig. 8b). This facies corresponds to sediment type A and B of Krajewski (2008).

Facies 2 (F2). This facies (Fig. 8a) is seen in the upper Muen Mb. (Fig. 3c), and in the lower and upper parts of the Blanknuten Mb. (Figs. 3d, 7a and 7b). It consists of laminated, black-colored mudstones and has mostly fissile weathering. Upon forced breakage, the fragments may appear both platy and flaky, but are typically harder and more brittle when compared to F1. The lamination planes are typically smooth, straight and parallel. Undulating laminae around phosphate nodules within this facies are common (Figs. 3d, 7a and 7b). These nodules partly represent phosphate-precipitated, filled burrows that are unlined, branched, and parallel to the bedding. This facies corresponds to sediment type C and E of Krajewski (2008).

Facies 3 (F3). This facies (Fig. 8a) occurs in the middle Blanknuten Mb. exclusively, and consists of finely laminated, black shales (Figs. 3e, 7c and 7d). Weathered sections are characterized by columnar, weather-resistant shale stacks in the outcrop face (Figs. 3a, 5b and 6b), forming the steepest cliff faces along outcrops of the Botneheia Fm., exemplifying the greatest weathering resistance among the mudstone facies (Figs. 4a and 5b). The lamination planes are mostly smooth, sharp, and parallel (Fig. 8a). Bioturbation and macroscopic phosphate nodules are virtually absent. This facies corresponds to sediment type D of Krajewski (2008), assigned to the phosphogenic succession (Fig. 3a).

Facies (F4). This facies occurs in the upper Blanknuten Mb. It is slightly brighter in color compared to F3 (Fig. 8a). Fragments may be highly fissile, but also calcareous and competent, resembling marlstone or limestone. Forced splitting of well-laminated samples generally reveals less mechanical competence and internal cohesion between laminae compared to F2 and F3. The plane texture between laminae is typically rougher than F2 and F3 (Fig. 8a). Mm-sized shell fragments are scattered throughout the matrix. Like F2, undulating laminae due to phosphate nodule precipitation are common. Filled, unlined, branched phosphate-precipitated burrows occur parallel to the bedding (Fig. 7e). Based on changes in hardness, lamination, color, texture and reaction to hydrochloric acid, this facies appears to contain significant internal variations in carbonate content, ranging from calcareous shales to impure limestones. The broad variations in detrital siliciclastic and calcite content denote this facies to represent varying combinations of sediment type C and G of Krajewski (2008).

4.3. Bulk elements

The lower–middle Muen Mb. consists of relatively low TOC values (median 1.42 ± 0.64 wt. %; Table 2) that are mostly stable throughout this part of the Botneheia Fm. (Fig. 9). All but one sample of the upper Muen Mb. show TOC of 4 wt. % or more (median 4.93 ± 1.75 wt. %) and marks the onset of a prominent positive TOC excursion that strongly contrasts the underlying strata (Fig. 9). An upwards increasing TOC trend is seen through the lower Blanknuten Mb. (median 5.36 ± 2.42 wt. %) until the middle Blanknuten Mb. (median 8.41 ± 1.93 wt. %) is reached (Fig. 9). From here, TOC decreases from the base upper Blanknuten Mb. (median 6.10 ± 2.30 wt. %) and upwards until the top formation boundary is encountered (Fig. 9). The TOC values for the Tschermakfjellet Fm. (median 1.76 ± 0.70 wt. %) are very similar to the lower–middle Muen Mb., both consisting of F1 mudstones (Fig. 8a; Table 2). These trends are valid for both the Blanknuten and Skrukkefjellet localities (Fig. 9).

The TIC content slightly increases from the lowermost Muen Mb. (median 1.36 ± 0.24 wt. %) and upwards until the top of the middle Blanknuten Mb. (median 2.30 ± 0.71) (Fig. 9). The upper Blanknuten Mb. shows a correlative, positive excursion in both localities, and the highest TIC content among the stratigraphic units (median 3.73 ± 1.61 wt. %). As with TOC, the TIC content in the Tschermakfjellet Fm. (median 1.43 ± 0.94 wt. %) is comparable to the lower–middle Muen Mb. (both F1 mudstones).

Table 2
Descriptive statistics of parameters derived from LECO and Iatroscan TLC-FID analyses for the defined stratigraphic units and facies, combining both localities. min = minimum, max = maximum, std = standard deviation (±1σ).

		Stratigraphic unit						Facies			
		lower-middle Muen Mb.	upper Muen Mb.	lower Blanknuten Mb.	middle Blanknuten Mb.	upper Blanknuten Mb.	Tschermakfjellet Fm.	F1	F2	F3	F4
	count	32	6	15	30	15	3	35	22	30	14
TOC (wt. %)	min	0.55	2.49	3.66	4.70	2.18	1.18	0.55	2.49	4.70	2.18
	median	1.42	4.93	5.36	8.41	6.10	1.76	1.44	5.16	8.41	6.04
	std	0.64	1.75	2.42	1.93	2.30	0.70	0.64	2.23	1.93	2.36
	max	3.92	7.78	12.03	11.61	11.84	2.58	3.92	12.03	11.61	11.84
TIC (wt. %)	min	0.87	0.99	1.12	0.76	1.94	0.11	0.11	0.99	0.76	1.94
	median	1.36	1.42	1.73	2.30	3.73	1.43	1.36	1.63	2.30	3.78
	std	0.24	0.31	0.46	0.71	1.61	0.94	0.33	0.47	0.71	1.60
	max	1.92	1.80	2.78	3.63	7.45	1.92	1.92	2.78	3.63	7.45
TS (wt. %)	min	0.35	0.75	0.66	0.53	0.38	0.04	0.04	0.66	0.53	0.38
	median	0.83	0.99	1.09	1.43	1.11	0.77	0.80	1.11	1.43	1.09
	std	0.27	0.34	0.30	0.67	0.60	0.57	0.30	0.43	0.67	0.46
	max	1.30	1.63	1.72	3.53	2.61	1.17	1.30	2.61	3.53	1.78
TOC/TS	min	0.78	3.17	2.75	1.98	1.71	2.21	0.78	2.75	1.98	1.71
	median	1.61	4.52	4.56	5.76	5.80	2.30	1.78	4.41	5.76	6.10
	std	1.00	1.57	3.08	2.44	4.56	17.66	5.31	2.71	2.44	4.58
	max	5.19	7.32	12.64	11.99	18.16	32.84	32.84	12.64	11.99	18.16
	Count	12	4	12	19	7	3	15	17	19	6
SAT (mg/g rock)	min	0.21	1.51	0.30	0.73	0.33	0.06	0.06	0.30	0.73	0.60
	median	0.75	2.44	1.62	1.64	0.80	0.22	0.52	1.63	1.64	0.87
	std	0.44	1.15	0.88	0.43	0.28	0.22	0.46	1.04	0.43	0.21
	max	1.70	4.05	3.33	2.20	1.18	0.50	1.70	4.05	2.20	1.18
ARO (mg/g rock)	min	0.03	0.91	0.27	0.64	0.11	0.04	0.03	0.27	0.64	0.11
	median	0.10	1.97	0.89	2.00	0.28	0.04	0.10	0.91	2.00	0.32
	std	0.08	0.61	0.97	2.18	0.21	0.07	0.08	0.92	2.18	0.23
	max	0.27	2.30	3.44	7.97	0.68	0.17	0.27	3.44	7.97	0.68
POL (mg/g rock)	min	1.05	4.88	4.39	6.02	4.14	1.91	1.05	4.39	6.02	4.14
	median	2.12	8.85	5.71	8.58	5.26	2.12	2.12	5.72	8.58	5.30
	std	1.00	2.93	1.96	2.20	1.34	0.72	0.93	2.34	2.20	1.40
	max	4.56	11.67	10.43	12.70	7.49	3.26	4.56	11.67	12.70	7.49
EOM (mg/g rock)	min	1.29	7.29	4.97	7.90	5.13	2.01	1.29	4.97	7.90	5.37
	median	3.02	13.26	8.77	12.84	6.25	2.39	2.76	8.96	12.84	6.30
	std	1.46	4.60	3.47	4.18	1.43	1.01	1.37	4.03	4.18	1.40
	max	6.45	18.02	17.20	21.71	8.76	3.92	6.45	18.02	21.71	8.76
EOM/TOC	min	0.17	0.15	0.07	0.10	0.07	0.14	0.14	0.07	0.10	0.08
	median	0.21	0.23	0.17	0.15	0.10	0.15	0.20	0.18	0.15	0.12
	std	0.03	0.05	0.07	0.04	0.07	0.02	0.04	0.07	0.04	0.07
	max	0.26	0.27	0.29	0.23	0.27	0.17	0.26	0.29	0.23	0.27
SAT (%)	min	16.07	16.43	6.11	7.05	6.36	3.05	3.05	6.11	7.05	8.08
	median	24.77	20.28	17.91	11.63	11.13	9.31	21.69	19.01	11.63	11.96
	std	4.54	2.55	6.17	3.20	4.59	4.90	7.72	6.04	3.20	4.20
	max	29.91	22.50	27.92	18.22	20.32	12.70	29.91	27.92	18.22	20.32
ARO (%)	min	2.08	12.47	5.48	6.75	1.83	1.74	1.74	5.39	6.75	1.83
	median	4.12	13.22	12.17	16.55	5.39	1.84	3.66	12.63	16.55	5.04
	std	2.06	1.81	5.06	9.54	2.98	1.45	2.03	4.68	9.54	3.26
	max	8.26	16.43	22.14	37.64	8.39	4.30	8.26	22.14	37.64	8.39
POL (%)	min	64.55	64.76	56.74	50.13	71.28	83.00	64.55	56.74	50.13	71.28
	median	72.29	66.64	69.47	71.22	82.91	88.86	73.66	67.11	71.22	82.03
	std	4.85	1.07	8.82	8.49	6.08	6.10	8.55	8.83	8.49	6.11
	max	81.48	67.15	88.41	84.00	89.57	95.21	95.21	88.41	84.00	89.57
SAT/ARO	min	3.14	1.00	0.52	0.19	1.18	1.75	1.75	0.52	0.19	1.37
	median	5.56	1.55	1.40	0.70	2.42	2.96	4.67	1.45	0.70	2.93
	std	3.78	0.34	0.68	0.60	2.45	1.68	3.73	0.59	0.60	2.48
	max	12.85	1.77	2.88	2.70	7.00	5.07	12.85	2.88	2.70	7.00

Except for a few excursions, the TS curve shows a similar trend as the TOC curves (Fig. 9), however with an overall lower range (0.04–3.53 wt. % in all samples; Table 2).

TS vs. TOC plots are commonly used to infer paleo-depositional environments focusing on benthic redox conditions (Alsenz et al., 2015; Berner and Raiswell, 1983; Smolarek et al., 2017). While this study does not distinguish pyritic versus kerogen sulfur, the results are comparable with the C/S systematics of Krajewski (2013, his Fig. 23). The inferred depositional environments denote oxic–suboxic benthic conditions for the lower–middle Muen Mb. and the Tschermakfjellet Fm. (both F1 mudstones) (Fig. 10). This greatly contrasts the upper Muen Mb. and the entire Blanknuten Mb. (consisting of F2, F3 and F4 mudstones) that generally plot below the normal marine line (Fig. 10).

4.4. Bulk bitumen distribution

Source rock extracts are often characterized using relative and absolute abundancy of saturates, aromatics, resins and asphaltenes (Tissot and Welte, 1984). Bitumen abundance or composition may be visually evaluated by variations in extract color (e.g., Abay et al., 2014; Matapour et al., 2019). The lower–middle Muen Mb. to the upper Muen Mb. boundary displays a strong change in extract hue from transparent cognac-like to opaque dark brown to black (Fig. 11) which imply richer extracts and/or more polar compounds above the F1–F2 boundary in the

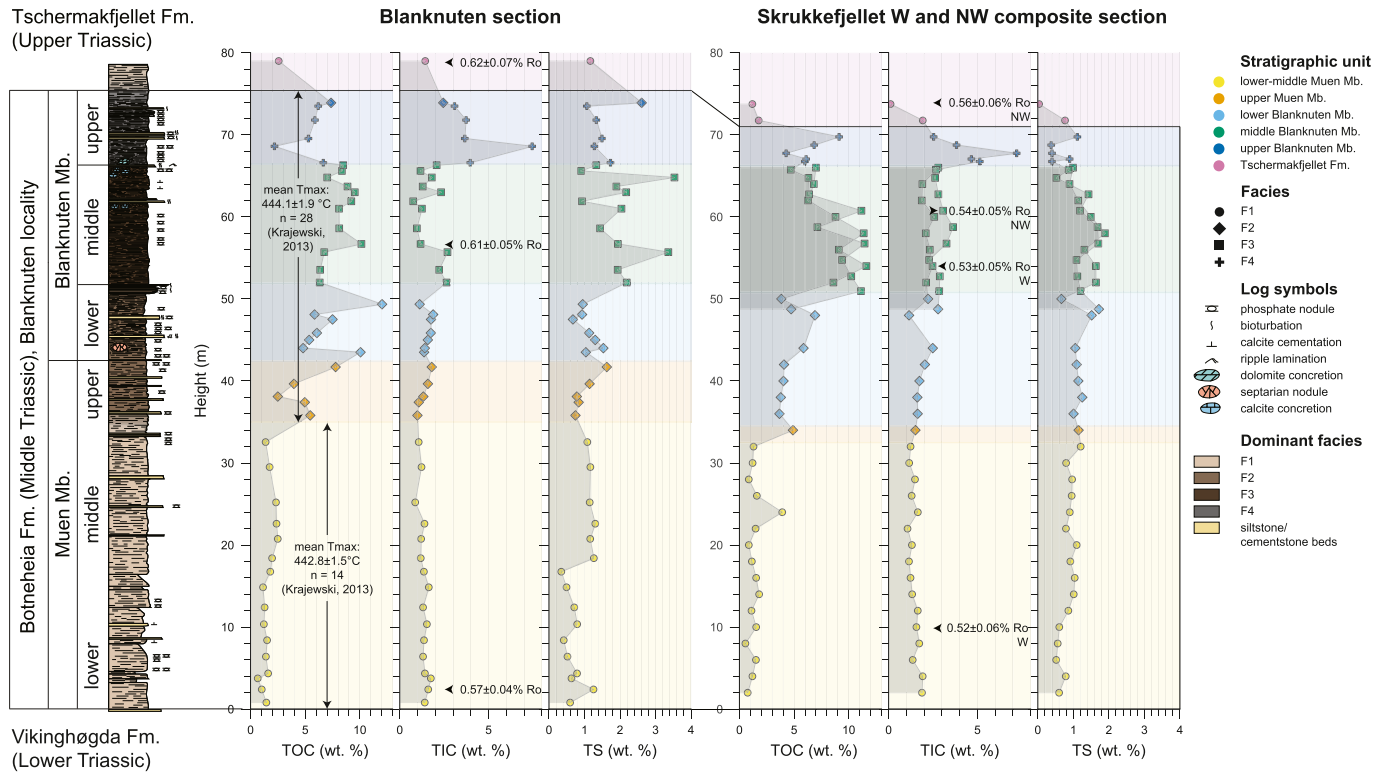

Fig. 9. Lithostratigraphic log from Blanknuten compared with LECO data (TOC, TIC, TS) and vitrinite reflectance from the Blanknuten section and Skrukkefjellet composite section. The lower and upper part of the two Skrukkefjellet logs are combined from the W and NW localities, resulting in overlap at level 49–66 m marked by darker shade of gray. The T_{max} values are taken from Krajewski (2013, his Appendix A) and represents samples from units 2–4 and units 5–8 in the in the Blanknuten locality respectively. (For interpretation of the references to color in this figure legend, the reader is referred to the Web version of this article.)

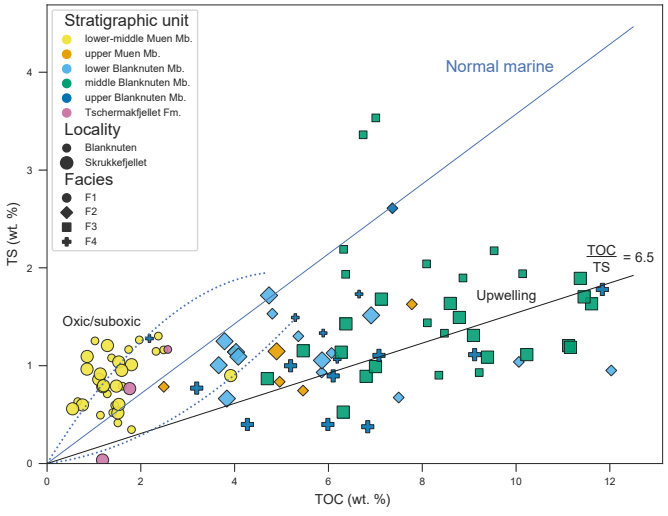

Fig. 10. Cross plot showing the relationship between TOC and TS. The blue line reflects the normal marine trend (Berner and Raiswell, 1983), while the dotted compartment shows typical distribution of normal marine samples (Berner and Raiswell, 1983; Leventhal, 1995). Areas indicating oxic/suboxic conditions and upwelling are retrieved from Ghassal et al. (2018) and Smolarek et al. (2017) respectively. (For interpretation of the references to color in this figure legend, the reader is referred to the Web version of this article.)

Muen Mb. The lower Blanknuten Mb. is not discernible from the upper Muen Mb. in agreement with both units consisting of F2 mudrocks. In contrast, all the extracts from the middle Blanknuten Mb. (F3) are black. The dark brown–black extracts from the upper Blanknuten Mb. samples are slightly brighter and comparable to the upper Muen Mb. and the lower Blanknuten Mb. The Tschermakfjellet Fm. in the Skrukkefjellet locality shows comparable brightness to the lower–middle Muen Mb. (both F1 mudstones), however the uppermost Tschermakfjellet Fm. sample from the Blanknuten locality is clearly darker. These visual properties generally match the quantitative TLC-FID chromatograms (Fig. 12).

The stratigraphic distribution of the total EOM in both study localities clearly shows relatively low but stable values in the lower–middle Muen Mb. that suddenly increase at the onset of the upper Muen Mb., in adherence to the F1–F2 facies boundary within this member (Fig. 13). A varying upwards EOM increase is seen within the upper Muen Mb. and the lower Blanknuten Mb., where these two units show maximum absolute SAT content in the Blanknuten (4.05 mg/g rock) and Skrukkefjellet (3.33 mg/g rock) localities respectively. Maximum EOM and absolute ARO values are encountered in the middle Blanknuten Mb. in both localities (Fig. 13). From here, the EOM content progressively decreases upwards into the upper Blanknuten Mb. and the Tschermakfjellet Fm., where the latter unit is comparable to the lower–middle Muen Mb. (both F1 mudstones). These trends correlate well with the TOC curve (Fig. 9).

The normalized SAT (%), ARO (%) and POL (%) fractions (Fig. 14) show that all samples are dominated by the POL (%) fraction, a common trait for source rock extracts (Le Tran and Philippe, 1993). The lower–middle Muen Mb. shows a dominance of SAT (%) content that progressively decreases through the upper Muen Mb. and the lower Blanknuten Mb., ultimately resulting in the lowest SAT (%) in the middle Blanknuten Mb. This distribution is mainly caused by a relative increase in aromatic hydrocarbons (HCs) rather than decreasing polar compounds (Table 2; Fig. 12). The upper Blanknuten Mb. and Tschermakfjellet Fm. show lowered SAT (%) and ARO (%), concurrently resulting in a dominating POL (%) fraction (Fig. 14).

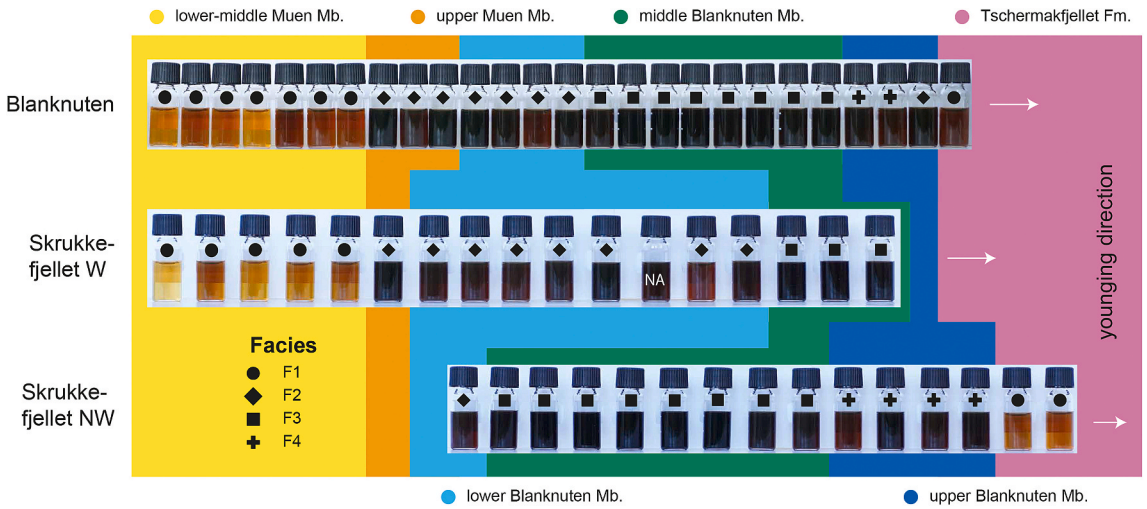

Fig. 11. Comparison of 2 ml vials containing extracts at equal dilution (3.85 vol % of original strength) against stratigraphic units. The sample labeled NA is not included in this study.

4.5. Thermal maturity and source facies

The vitrinite reflectivity data (Fig. 9) indicates that the Botneheia Fm. in the Blanknuten locality (mean R_o = 0.60%) and in the Skrukkefjellet composite section (mean R_o = 0.54%) are dominantly early mature and immature respectively (cf. Peters and Cassa, 1994). The Skrukkefjellet W and NW localities show virtually identical maturities. The vitrinite values in each of the Blanknuten and Skrukkefjellet localities overlap regardless of sample elevation (Fig. 9) inferring a negligible maturity gradient with depth for each locality but a lateral maturity contrast between these localities.

The SAT/ARO and EOM/TOC ratios of source rock extracts are expected to increase with increasing thermal maturation (Law, 1999; Peters and Cassa, 1994). This is because kerogen and bitumen are cracked into saturate HCs rather than aromatic HCs with increasing maturity, resulting in the relative decrease of aromatic compounds respective to saturates and thus increasing the ratio. However, the SAT/ARO ratio is also affected by organofacies (Waples and Curiale, 1999) and weathering effects (Forsberg and Bjorøy, 1983), which might overprint any maturity signature. Similarly, the EOM/TOC ratio is expected to increase with increasing maturity, as kerogen crack into bitumen with increasing maturity (Peters and Cassa, 1994), but is similarly affected by organofacies and weathering.

The lower–middle Muen Mb. shows the highest SAT/ARO ratios (max 12.85), which may decrease up to an order of magnitude into the upper Muen Mb. (min 1.00) (Fig. 15; Table 2). These contrasting values form a chemostratigraphic boundary that conforms to the F1–F2 boundary in the Muen Mb. SAT/ARO ratios further decrease upward through the lower Blanknuten Mb. and into the middle Blanknuten Mb. The latter unit shows the minimum SAT/ARO ratios in both localities, which concurrently increases upwards into the upper Blanknuten Mb. and the Tschermakfjellet Fm. These two units show comparable SAT/ARO ratios (Fig. 15; Table 2). As there is no clear shift in SAT/ARO ratios comparing the Blanknuten and Skrukkefjellet localities with each other, it is not possible to apply this ratio as a maturity parameter to distinguish the proven maturity difference between these localities.

The EOM/TOC logs do not follow the same trends as the SAT/ARO logs (Fig. 15). This is shown by the highly variable and overlapping EOM/TOC values between all the stratigraphic units and associated facies for both sections (Fig. 15). Still, the lower–middle Muen Mb. shows overall higher EOM/TOC ratios compared to the middle Blanknuten Mb. in the Blanknuten section (median 0.21 ± 0.03 vs. median 0.13 ± 0.05) and the Skrukkefjellet composite section (median 0.20 ± 0.02 vs. median 0.17 ± 0.03). These EOM/TOC ratios alone give the impression that the middle Blanknuten Mb. in the Skrukkefjellet locality is more mature compared to the same unit in the Blanknuten locality, which is clearly false (Fig. 9). This parameter is therefore not reliable as a maturity indicator.

TOC content alone is not sufficient to determine source rock potential (Dembicki, 2009), but combined with EOM content, it is possible to evaluate gas-prone vs. oil-prone hydrocarbon generation potential (Fig. 16) (Dembicki, 2017; Le Tran and Philippe, 1993). The lower–middle Muen Mb. shows considerable variation and includes samples with the lowest oil potential in the sample set (Fig. 16). The upper Muen Mb. marks a prominent increase and plots similarly as the lower Blanknuten Mb., while the middle Blanknuten Mb. appears to reflect the most oil-prone unit (Fig. 16). The upper Blanknuten Mb. shows comparable oil potential as the lower Blanknuten Mb. The three Tschermakfjellet Fm. samples (i.e. strongly limited dataset) show EOM content >2 mg/g rock and TOC content >2 wt. % (Fig. 16), which is considered very good petroleum potential for immature source rocks (Peters and Cassa, 1994).

4.6. Exploratory data analysis

The principal component analysis (PCA) shows that 74.4% of the variance can be explained by principal components (PCs) 1 and 2 (Fig. 17). The lower–middle Muen Mb. correlates the most with elevated SAT/ARO ratio and SAT (%) content, and least with TOC, TS, and absolute ARO and POL content. The upper Muen Mb. shows grouping tendencies with the lower Blanknuten Mb. due to elevated absolute SAT concentrations, although the latter unit displays prominent scatter for both PCs. The middle Blanknuten Mb. (F3) correlates best with absolute ARO, POL, EOM and TOC content, and shows the greatest contrast to the lower–Middle Muen Mb. The upper Blanknuten Mb. is distinguished by relatively high content in polars, and overall low EOM/TOC. The samples from the Tschermakfjellet Fm. do not overlap with the other samples, but group between the lower–Middle Muen Mb. and the upper Blanknuten Mb.

From the hierarchical cluster analysis (HCA), five clusters (C1–C5) were identified (Fig. 18).

Cluster 1 (C1). This cluster consists of a single Tschermakfjellet Fm. F1 sample in the top Skrukkefjellet composite log (Fig. 9). This sample shows the greatest cluster distance and thus the least similarity with the remaining sample set (Fig. 18). This distinction is based on relatively low abundance in almost all the geochemical variables and especially the ARO (%) fraction (1.74%), resulting in a

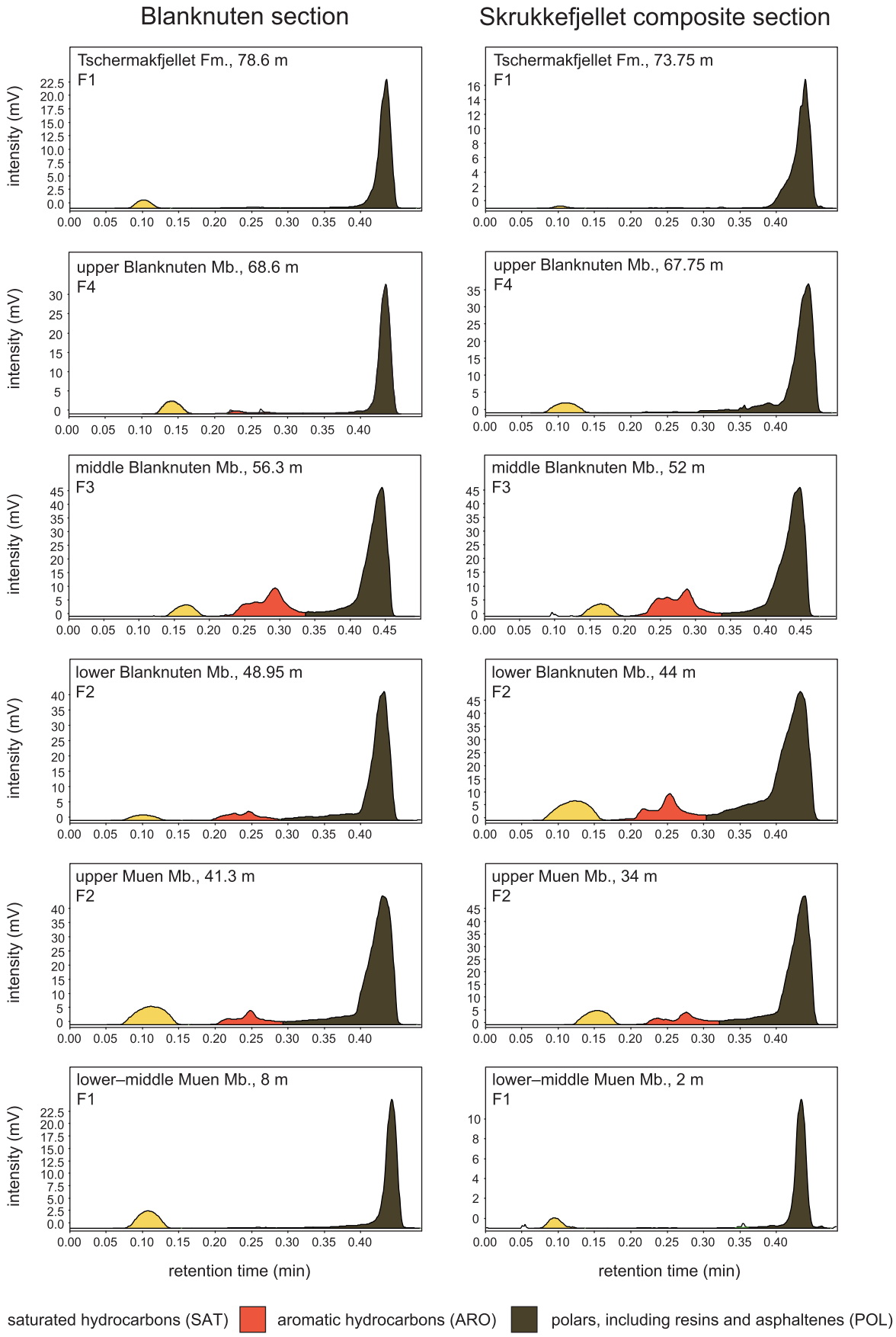

Fig. 12. Iatroscan chromatograms from each stratigraphic unit in both the Blanknuten and Skrukkefjellet localities. Note the overall absence of aromatic HCs in the lower–middle Muen Mb. and the Tschermakfjellet Fm. (both F1 mudstones).

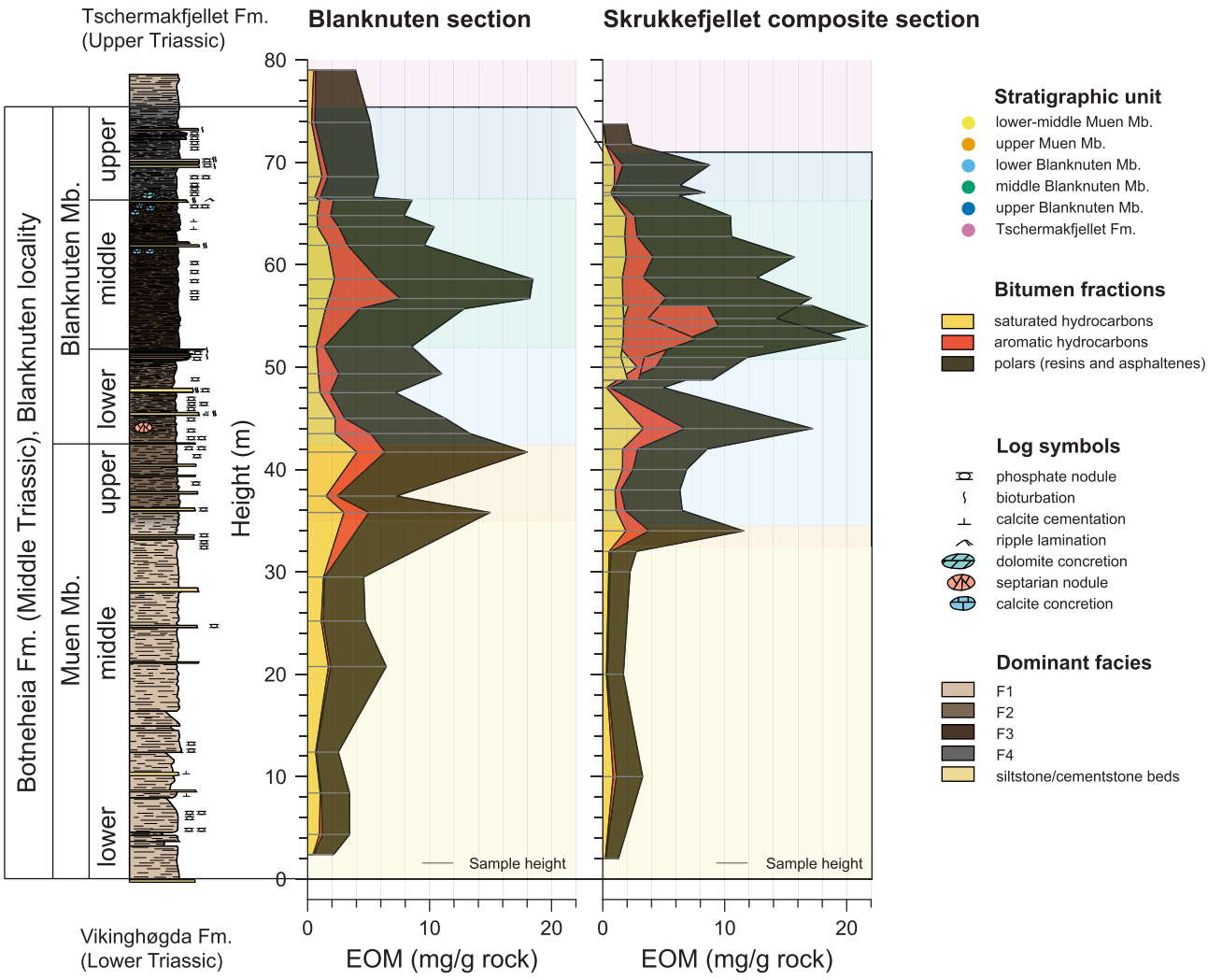

Fig. 13. Lithostratigraphic log from the Blanknuten locality compared with Iatroscan-derived EOM logs of the Blanknuten section and Skrukkefjellet composite section. The EOM content between the sample positions, as denoted by horizontal lines in the EOM logs, is linearly interpolated.

high POL (%) fraction (95.21%). TOC/TS is extremely high (32.84), and deviates substantially off the median (1.78) for F1 mudstones.

Cluster 2 (C2). This cluster contains nine samples representing F2 mudstones from the upper Muen Mb. and the lower Blanknuten Mb, but dominantly middle Blanknuten Mb. F3 mudstones (Fig. 18). C2 is recognized by high contents of TOC (5.46–11.61, median 8.60 wt. %), absolute POL (7.73–12.70, median 10.60 mg/g rock), ARO (2.06–7.97, median 4.08 mg/g rock) and EOM (13.16–21.71, median 18.02 mg/g rock). ARO (%) and POL (%) are relatively high (12.74–37.64, median 30.30%) and low to intermediate (50.13–68.78, median 60.67%) respectively (Fig. 14).

Cluster 3 (C3). This cluster represents 14 samples consisting of F1 mudstones only (i.e. the lower–middle Muen Mb. and Tschermakfjellet Fm.). It is characterized by low TOC (0.75–2.58, median 1.52 wt. %), TOC/TS (0.78–3.63, median 1.91), POL (1.05–4.56, median 2.14 mg/g rock), and EOM (1.29–6.45, median 3.02 mg/g rock). SAT (%) (9.31–29.91, median 22.64%) and POL (%) (64.55–88.86, median 73.21%) are both relatively high. This results in the highest SAT/ARO ratios (2.96–12.85, median 4.87) among all the clusters (Fig. 18).

Cluster 4 (C4). This cluster contains 29 samples including the upper Muen Mb. (F2) and the lower, upper and middle Blanknuten Mb. (F2–F4). C4 exhibits a complex relationship between all variables, leading to difficulties towards finding general geochemical systematics. However within the cluster, the two upper Muen Mb. samples (F2) clearly group with the five lower Blanknuten Mb. samples. These seven samples are stratigraphically close (Fig. 9) and of the same F2 mudstones (Fig. 18).

Cluster 5 (C5). This cluster contains four samples from the upper Blanknuten Mb. only. It is recognized by high TIC (4.66–7.45, median 6.17 wt. %) (Fig. 9), high POL (%) (71.28–89.57, median 84.15%), and high SAT/ARO ratios (2.42–7.00, median 4.94).

5. Discussion

The presented geochemical log panels of the Blanknuten and Skrukkefjellet localities are the first attempt at stratigraphically correlating and comparing carbon, sulfur and bulk bitumen content to described mudstone facies of the Botneheia Fm. and correlate these parameters against the regional Middle Triassic lithostratigraphic framework provided by Krajewski (2008). Given the significance and regional distribution of Early–Late Triassic organic rich deposits, the presented geochemical logs and correlations provide new insights in how the elemental and bitumen composition is tied to mudstone facies and stratigraphic units of the Botneheia (Anisian–Ladinian) and Tschermakfjellet (Carnian) fms. in Svalbard.

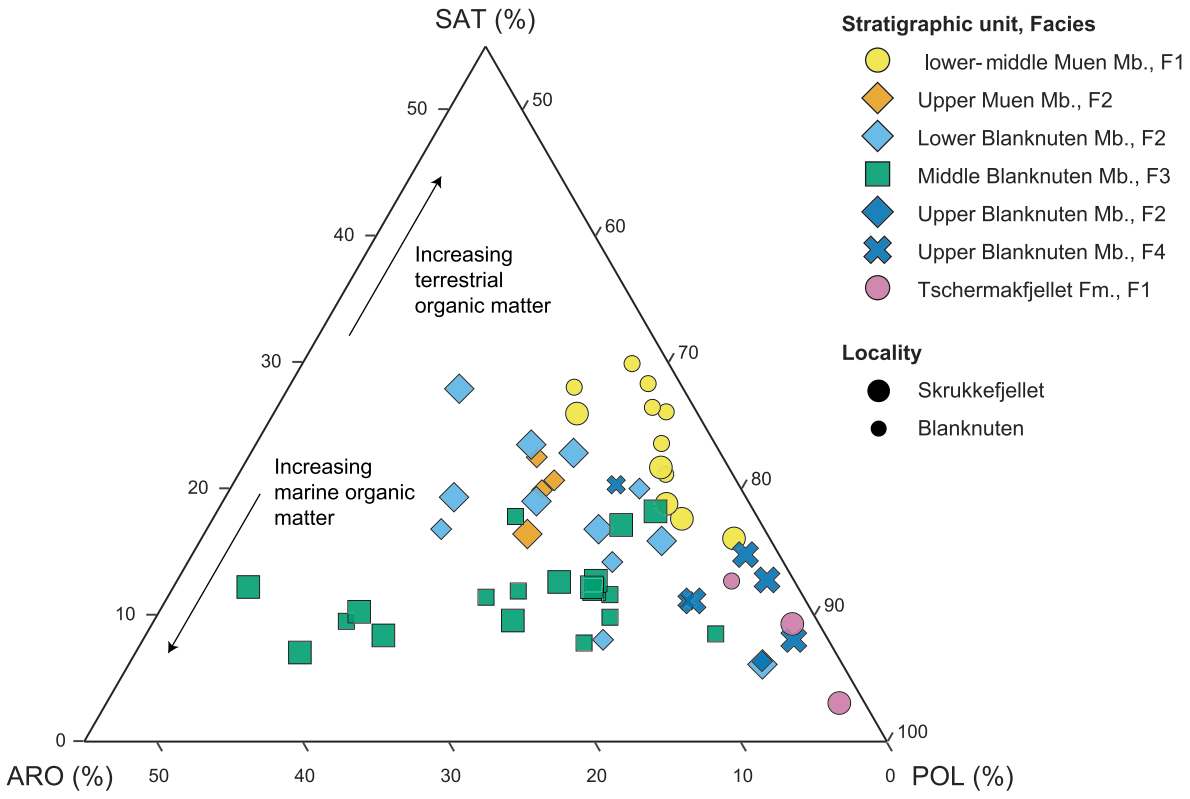

Fig. 14. Ternary plot of the bulk SAT (%), ARO (%) and POL (%) fractions (including resins and asphaltenes) normalized to 100% by weight. A greater content of SAT (%) in respect to ARO (%) indicates increased content of terrestrial relative to marine organic matter and vice versa (Tissot and Welte, 1984).

5.1. Challenges in estimating formation thickness and correlating lithostratigraphic sub-units

In this study, the basal boundary of the middle Blanknuten Mb. is placed at level c. 51–52 m in each study locality (Fig. 9). According to Mørk et al. (1999) and Vigran et al. (2008), the base of the Blanknuten Mb. is placed at c. 53 and 55 m height in the same localities. Thus, their base Blanknuten Mb. boundary can only correspond with the base of the middle Blanknuten Mb. of Krajewski (2008) and this study. The lower boundary of the Blanknuten Mb. was initially defined as the base of a calcareous, cliff-forming siltstone unit occurring within the upper part of Botneheia Fm. (Mørk et al., 1999). Later work by Krajewski (2008) identified the lower boundary of the Blanknuten Mb. at the base of cliff−forming mudstones and shales in the upper part of the Botneheia Fm. However, this definition may be too ambiguous. For instance, in steeper outcrops, the base of the lower Blanknuten Mb. acts as the onset of the so-called "Blanknuten Mb. cliff" (Fig. 3a), while in outcrops with gentler slope gradients, the base of the "Blanknuten Mb. cliff" starts at the base of the middle Blanknuten Mb., i.e. a younger stratigraphic level than in steeper sections (Figs. 4a and 5b). Thus, we emphasize that the *earliest* occurrence of F2 mudstones that show a remarkable increase in cliff-forming capability (Fig. 3a) should be considered as the base Blanknuten Mb., adhering to the boundary as defined by Krajewski (2008, his Fig. 4).

Source rock thickness is required to determine the source potential index (Demaison and Huizinga, 1991) and is therefore a crucial parameter for determining petroleum expulsion from source rocks. In central Spitsbergen, the formation thickness may be difficult to measure due to structural thickening (e.g. Haremo et al., 1990). Such effects are negligible on Edgeøya. Mørk et al. (1982) and Krajewski (2008) report a Botneheia Fm. thickness of c. 75 m and 101 m in the Blanknuten locality respectively. Krajewski (2008) reports a thinning of the Botneheia Fm. from the Blanknuten locality to the Skrukkefjellet locality, a distance of c. 20 km (Fig. 1b), while Vigran et al. (2008) report a formation thickness of c. 84 m in the Skrukkefjellet locality, i.e. a slight thickening of the Botneheia Fm. along the same trajectory. This study demonstrates that the formation thickness is generally the same in both localities (Fig. 9). The thickness difference of c. 5 m between the study localities might simply be due to the nature of the meter stick measurements, where a ±5 m error margin is realistic. If the measured thicknesses represent the true thicknesses, the thinning trend from south to north is in agreement with Krajewski (2008), however, the thickness estimates (Fig. 9) correspond much better with Mørk et al. (1982) and Vigran et al. (2008). A Botneheia Fm. thickness substantially above c. 85 m therefore appears unlikely on Edgeøya, in disagreement with Krajewski (2008, 2013). Thickness measurements retrieved from structure-from-motion drone surveys (e.g. Buckley et al., 2019) could provide a more accurate answer.

The facies change from lower–middle Muen Mb. F1 mudstones to upper Muen Mb. F2 mudstones occurs at level c. 33 m in both the Blanknuten and Skrukkefjellet sections (Fig. 9). Two tightly spaced siltstone layers at level 33 m in the Blanknuten section (Fig. 9) also occur at level 32 m in the Skrukkefjellet W section (not shown). Thus, the tub-like concretion in the Skrukkefjellet W section (Fig. 4c), which currently is assigned to the lower Blanknuten Mb. (Krajewski, 2008; Vigran et al., 2014), may instead belong to the phosphogenic F2 mudstones of the upper Muen Mb. We find it curious that the combined thickness of the upper Muen Mb. and the lower Blanknuten Mb. in the Blanknuten locality (c. 17 m; Fig. 9) and the Skrukkefjellet locality (c. 18 m; Fig. 9) is almost identical in both localities. Still, lateral facies variations should be expected (Krajewski, 2013).

A laterally extensive marker bed (highlighted blue text and arrow) marks the base of continuously competent F2 mudstones in the lower Blanknuten Mb. (Figs. 4a, 5a and 6a). This marker bed occurs c. 10 m above the currently defined base of the lower Blanknuten Mb. in the Skrukkefjellet locality (Fig. 9). If the base lower Blanknuten Mb. boundary was placed at the top of this bed, a good match in the Muen Mb. thickness and geochemical parameters between the localities would

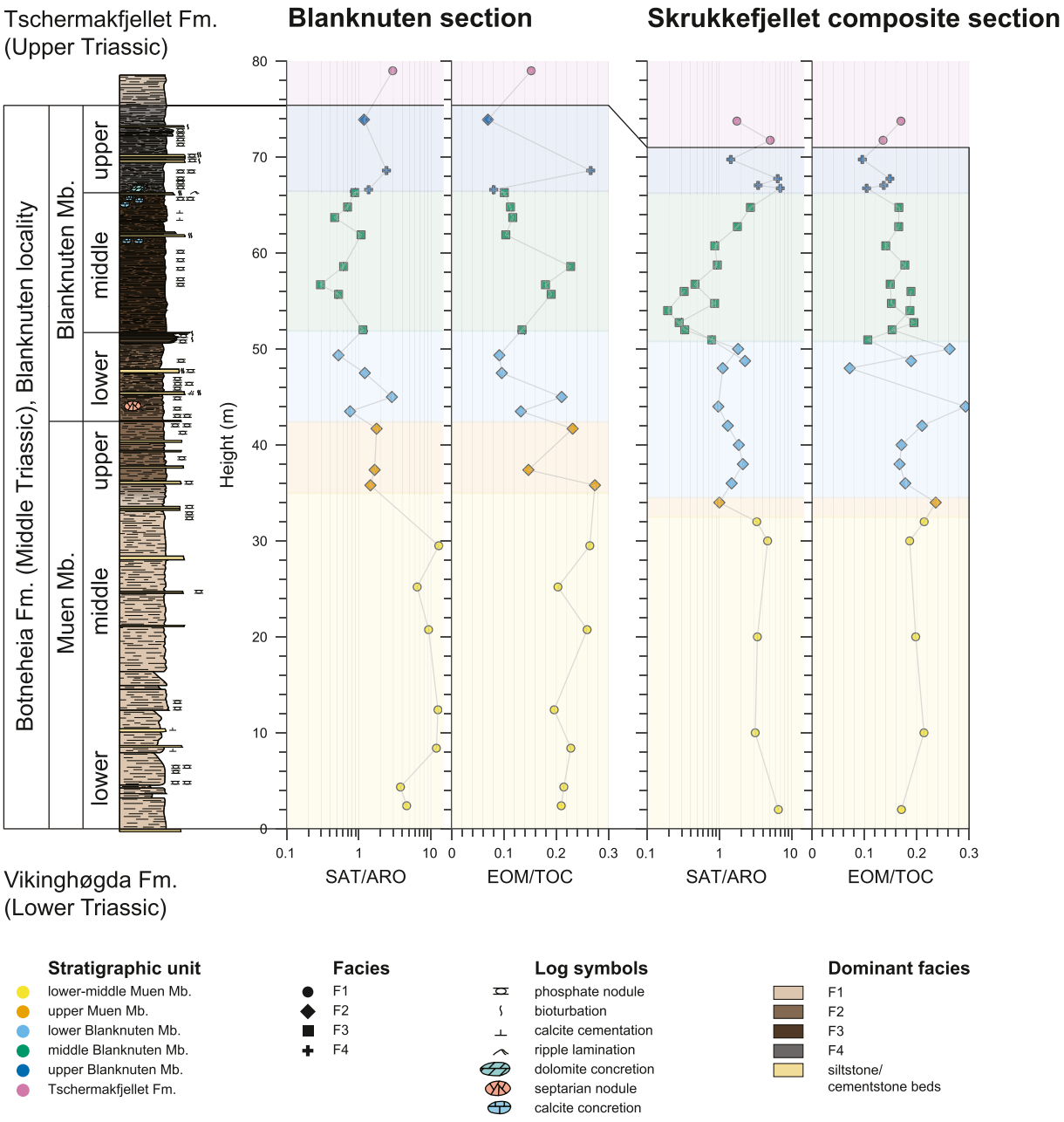

Fig. 15. Lithostratigraphic log from the Blanknuten locality compared with LECO and Iatroscan-derived geochemical logs from the Blanknuten and Skrukkefjellet localities.

be met (Figs. 9, 13 and 15). Still, as the upper Muen Mb. and the lower Blanknuten Mb. both consist of F2 mudstones and display comparable bulk geochemical assemblages (Figs. 17 and 18), their lithostratigraphic distinction appears less important for source rock characterization.

5.2. *Relating mudstone facies to depositional conditions*

Vigran et al. (2014) reported the entire Muen Mb. on Edgeøya to represent deposition during dominantly anoxic conditions based on pelagic fossil content and lack of bioturbation. However, the gray color and the presence of trace fossils within the lower–middle Muen Mb. F1 mudstones (Fig. 8) suggest that burrowing occured after deposition. The flaky weathering of these F1 mudstones (Fig. 3b) indicates a lack of laminae (cf. Potter et al., 2005) that may represent thorough matrix homogenization by biogenic reworking (Byers, 1974). Alternatively, the homogeneous matrix may reflect rapid deposition by low-density, mud-rich turbidity currents (Traykovski et al., 2000), fluid mud migration (Ruttenberg and Goni, 1997), or fallout from hypopycnal plumes (Schieber, 2016; Wilson and Schieber, 2014).

The mm-scale, sub-vertical burrows in the lower–middle Muen Mb. F1 mudstones are interpreted to be small-scale *Chondrites* trace fossils (Fig. 8b). These appear to be monogeneric and may indicate anoxic or possibly dysoxic benthic conditions (Bromley and Ekdale, 1984). However, a study on the Kimmeridge Clay Fm. reports *Chondrites* trace fossils in upper dysaerobic facies and not in the anaerobic facies (Wignall, 1991). *Chondrites* might also represent opportunistic exploitation of deeper, anoxic beds with oxygenated sea floor conditions (cf. Vossler and Pemberton, 1988). Consequently, these trace fossils are not clearly indicative of anoxic bottom conditions.

The unbranched, winding trails are interpreted to be *Helminthopsis* trace fossils (Fig. 8b) and provide evidence of a habitable sea floor. The co-occurrence of *Chondrites* and *Helminthopsis* trace fossils and the gray

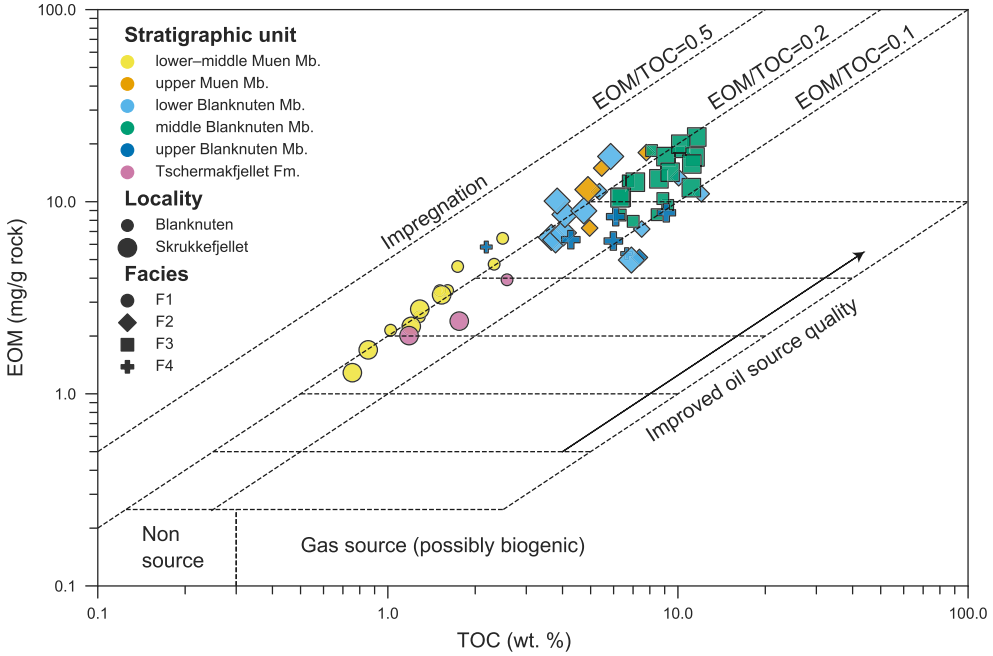

Fig. 16. Cross plot of TOC (wt. %) versus total EOM (mg/g rock). The inferred zones are adapted from Le Tran and Philippe (1993).

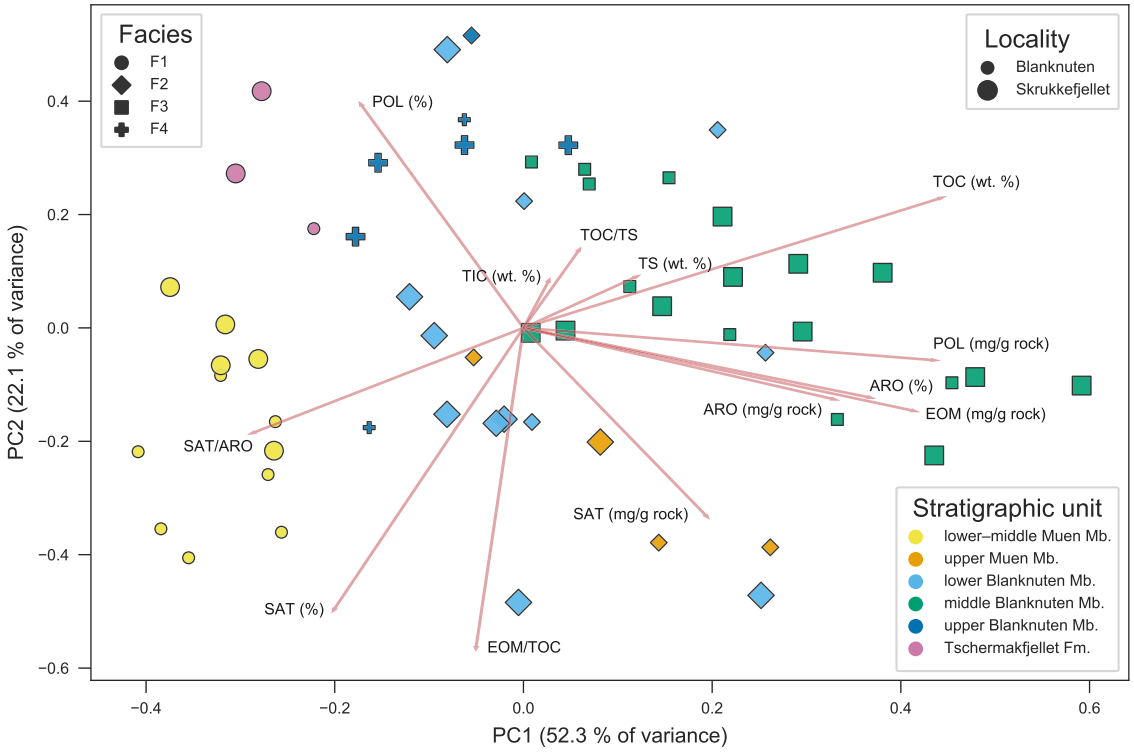

Fig. 17. Combined PCA score plot and loading plot of 13 variables derived from 57 samples. The loadings (red arrows) are normalized by the largest range in each PC. (For interpretation of the references to color in this figure legend, the reader is referred to the Web version of this article.)

color of the lower–middle Muen Mb. F1 mudstones indicates oxic–dysoxic bottom conditions (MacEachern et al., 2009). The low abundance of macroscopic trace fossils might indicate benthic soup-ground conditions during deposition as such conditions are biased against the preservation of soft biogenic structures (MacEachern et al., 2009). However, microscopic investigations by Krajewski (2013) show that the lower–middle Muen Mb. is bioturbated as a rule and suggest that the benthic conditions were dominantly oxic.

Recent work on the Tschermakfjellet Fm. on Edgeøya (i.e. F1 mudstones in this study) report on *Helminthopsis* trails within the mudstones facies of this unit and interpreted this facies to represent low-energy, offshore to distal pro-delta suspended load deposits (Anell et al., 2020). Similarly, Krajewski (2013) denotes the F1 mudstones in the lower–middle Muen Mb. to represent pro-deltaic to open shelf deposits.

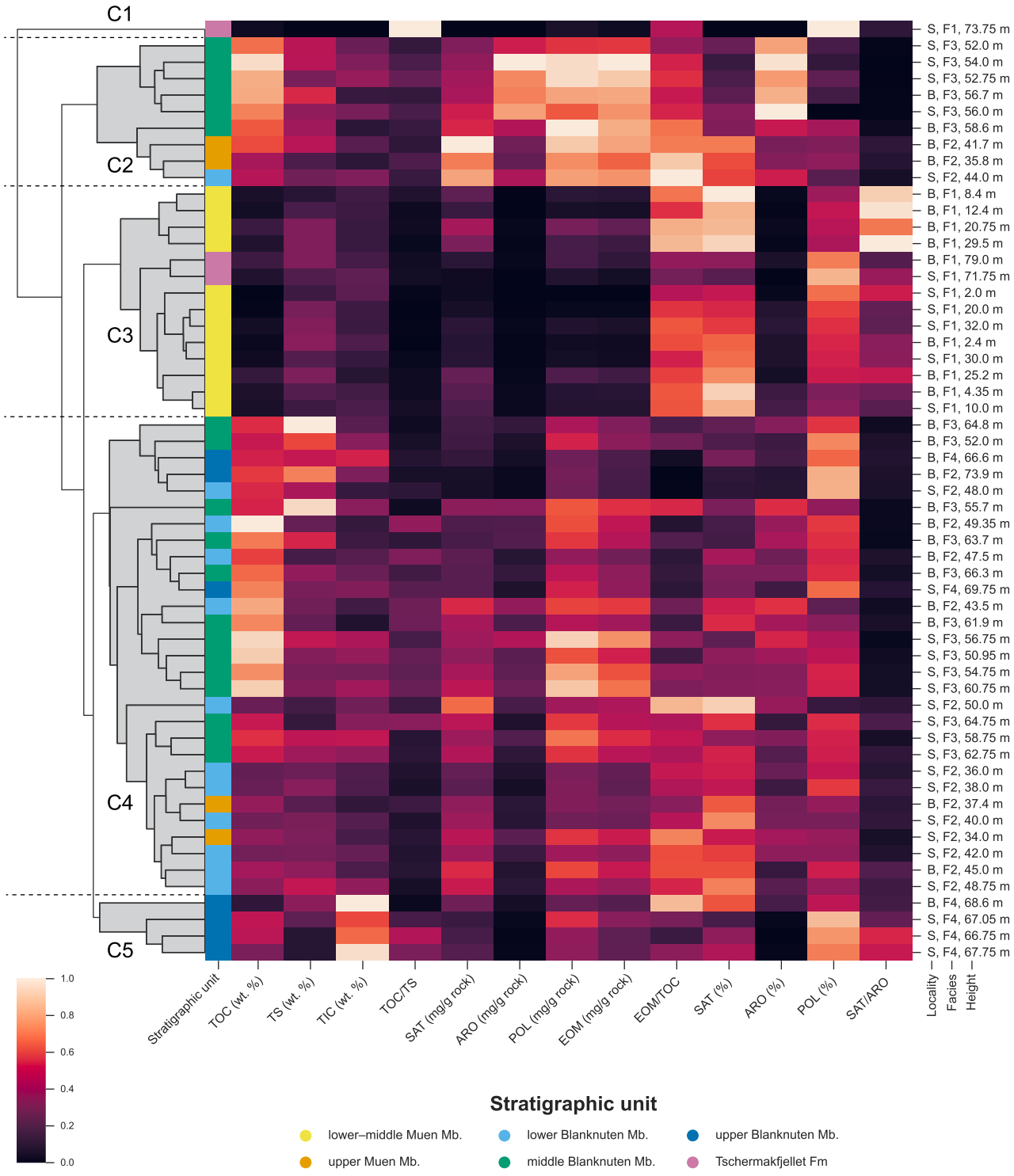

Fig. 18. Combined HCA dendrogram and heatmap of 13 variables (columns) derived from 57 samples (rows) from the Blanknuten and Skrukkefjellet localities. The heatmap and associated color map represents the rescaled [0, 1] values of each variable. B and S represents Blanknuten and Skrukkefjellet localities, respectively. (For interpretation of the references to color in this figure legend, the reader is referred to the Web version of this article.)

This correlation between the F1 mudstones from the lower–middle Muen Mb. and the Tschermakfjellet Fm. suggests that these stratigraphic units were deposited in similar depositional settings. A dominantly deep, restricted and anoxic shelf setting for the lower–middle Muen Mb. F1 mudstones as suggested by Lundschien et al. (2014, their Fig. 7) and Vigran et al. (2014) therefore seems questionable.

The oxygenated conditions in the lower–middle Muen Mb. might be related to the distal regressive phase conforming to the Anisian–Ladinian TR-cycle seen in the time-equivalent Bravaisberget Fm. in western Spitsbergen (Mørk et al., 1989). This could explain the relative abundance of carbonate cemented siltstone beds in the upper Muen Mb. compared to its lower part (Figs. 3a and 9). The base Anisian transgression could also have flooded the Svalbard Platform and created hydrodynamic configurations that allowed benthic ventilation and

oxygenation. This mechanism was initially suggested as an explanation for the well-ventilated conditions that followed the base Carnian transgression (Høy and Lundschien, 2011).

The well preserved laminae, increased brittleness and dark color of F2 mudstones (Figs. 3c and d, 7a–b, 8a) are interpreted to represent less or no bioturbation due to decreased oxygen levels, thus favoring organic matter preservation (Demaison and Moore, 1980). In addition, phosphogenesis in marine sediments, as evidenced by phosphate nodules (Figs. 3d, 7a–b), is commonly associated with a continental shelf to slope environment with high organic productivity induced by upwelling, low detrital input, and periodic winnowing and reworking (Arthur and Sageman, 1994; Demaison and Moore, 1980; Filippelli, 2011). The increased brittleness is likely to represent the sudden increase in both TOC and TIC content (Fig. 9), as both kerogen and calcite cement may act as binders causing brittle shales (Krajewski, 2008; Potter et al., 2005). The burrows (Fig. 9) indicate occasionally hospitable benthic conditions. The first occurrence of this facies may represent the earliest phosphogenic mudstones in eastern Svalbard (Krajewski, 2008). However, the F1–F2 boundary at level 35 m (Fig. 9) in the Blanknuten locality does not directly correspond to the non-phosphogenic–phosphogenic boundary within the Muen Mb. as defined by Krajewski (2008, 2013). Using Fig. 9 in this study as a height reference, Krajewski (2008, his Fig. 3a; 2013, his Fig. 3b, d) defined the non-phosphogenic–phosphogenic boundary in the Blanknuten locality to be at level c. 29 m and 25 m respectively. These inconsistencies make it challenging to determine the true stratigraphic level of the non-phosphogenic–phosphogenic boundary in the Muen Mb.

The F3 mudstones (Fig. 7c and d) are characterized by the best-preserved laminae among all the facies, absent bioturbation, darkest color (Fig. 8a), highest TOC (median 8.41 wt. %) and greatest brittleness. F3 is interpreted to be deposited during oxygen-depleted conditions with absent macroscopic bioturbation, contrasting the underlying F1 and F2 mudstones. The elevated brittleness is likely a result of the increased TOC and TIC cementation (Fig. 9). The F3 mudstones are exclusive to the middle Blanknuten Mb. (Fig. 3a), and this unit probably reflects the most stable depositional conditions among the described facies as it displays only two high-energy, macroscopic event beds and shows an overall homogenous sedimentary log (Fig. 9). However, Vigran et al. (2008) reported abundant *Daonella* bivalves in the middle Blanknuten Mb. in the Skrukkefjellet locality, indicating that the sea floor was occasionally inhabited, i.e. not permanently anoxic (Schatz, 2005). Similar observations were made by Alsen et al. (2017) for the equivalent Israd Fm. in the Wandel Sea Basin, northeastern Greenland. Krajewski (2013) shows frequent microscopic packstone layers within F3 mudstones in the middle Blanknuten Mb., reflecting that bottom waters cannot have been permanently stagnant, in agreement with the two macroscopic event beds (Fig. 9). This suggests that high primary productivity rather than water mass restriction introduced by bathymetric relief was the main driver for oxygen depletion and subsequent benthic preservation potential (cf. Ghadeer and Macquaker, 2012). Krajewski (2013) argues that a submarine swell c. 50 km N–NE of the Blanknuten locality contributed to water mass restriction during the deposition of F3 mudstones, as he did not observe this facies there. Based on the paleogeographic setting, Høy and Lundschien (2011) conclude that a halocline triggered by abundant fresh water and nutrient supply from the southwestern delta system with subsequent primary production was more important than bathymetric relief for organic matter preservation in the bulk Botneheia Fm.

Based on the dark color and high TOC (median 6.10 wt. %), the F4 mudstones (exclusive to the upper Blanknuten Mb.) are interpreted to be deposited during mainly oxygen-depleted conditions caused by high primary productivity. However, abundant macroscopic, coarser-grained event beds and phosphate-filled burrows (Figs. 3f, 5d, 7e–f) indicate high-energy deposits and oxygenation episodes. The sudden increase in TIC also demarcates this facies from the underlying F3 mudstones (Fig. 9). The TIC content is linked to the abundance of shell fragments in the F4 mudstones, increasing in concert with its mechanical competency. This is expressed in the Skrukkefjellet locality, where the base of the upper Blanknuten Mb. is more cliff-forming than the underlying top middle Blanknuten Mb. (Fig. 5d). The TIC excursion therefore acts as a marker horizon in delineating the underlying F3 dominated source rock unit and the above F4 dominated source rock (Fig. 9). These observations and descriptions support the observations of Krajewski (2008) and Mørk and Bromley (2008), who interpreted the F4 mudstones to represent regional regressive deposits, with interchanging hospitable–unhospitable benthic conditions.

Three factors have been extensively debated in terms of their significance in forming organic-rich sedimentary successions, i. e. (i) organic productivity (Pedersen and Calvert, 1990); (ii) organic-matter preservation (Demaison and Moore, 1980); and (iii) sedimentation rate (Creaney and Passey, 1993). From the discussion above, it appears that oxygen depletion due to high primary productivity coupled with condensation caused by increased relative sea level are important factors contributing to the organic richness in the Botneheia Fm. in eastern Svalbard. Water mass restriction as a result of paleobathymetric configuration seems less important, given the implied oxic conditions during the Anisian (F1 mudstones, lower–middle Muen Mb.).

5.3. Defining normal marine vs. upwelling conditions by TOC/TS systematics

TOC/TS ratios are higher in sediments deposited in upwelling zones than those deposited under normal marine settings (Morse and Emeis, 1990). The relatively low TOC/TS ratios in the lower–middle Muen Mb. (median 1.61) and the Tschermakfjellet Fm. (median 2.30) (both F1 mudstones) are representative of normal marine conditions with oxic to slightly dysoxic bottom waters (Fig. 10) (cf. Ghassal et al., 2018). In contrast, the TOC/TS ratios in the upper Muen Mb. (median 4.52) and the lower, middle and upper Blanknuten Mb. (median 4.56, 5.76 and 5.80 respectively) indicate conditions that are consistent with high primary productivity and possibly upwelling (Fig. 10). Greater TOC/TS ratios might reflect regularly ventilated seafloor conditions (Smolarek et al., 2017), as pyrite is oxidized more rapidly than organic matter (Marynowski et al., 2011). The reported oxygenation events during deposition of the Blanknuten Mb. could deplete sulfur more readily than organic carbon and thus preserve organic matter. The very low TS in the uppermost Tschermakfjellet Fm. sample in the Skrukkefjellet locality (minimum 0.04 wt. %) (Fig. 9) could indicate intense TS depletion caused by a well-ventilated and oxic depositional environment.

Alsenz et al. (2015) assigned a TOC/TS ratio of 6.5 in the Maastrichtian Ghareb Fm. (Negev, Israel) to upwelling conditions, which overlaps with the entire Blanknuten Mb. but mostly its middle and upper part (Fig. 10). Alsenz et al. (2015) concluded that low iron availability promoted sulfur incorporation into the organic matter, preserving the-organic matter against microbial degradation. The iron content has previously been reported to be lower for the Blanknuten Mb. compared to the Muen Mb. (Krajewski, 2013). The distal parts of the Triassic Boreal Sea were sediment starved during the Ladinian transgression (Klausen et al., 2015) and the distal shelf setting likely received less detrital iron and perhaps fluvial-sourced nutrients. In Svalbard, Anisian sedimentation rates were higher than Ladinian (Hounslow et al., 2008). Thus, Svalbard most likely received more detrital iron content during the Anisian than in the Ladinian.

5.4. Main influences on bitumen quantity and composition

Bitumen represents a continuum of compounds, from simple, straight *n*-alkanes to large and complex asphaltenes (Redelius and Soenen, 2015). It is therefore challenging to deconvolute the influence of organofacies, thermal maturity, and biodegradation, which are the most important factors affecting the composition of petroleum fluids (England and Mackenzie, 1989). Outcrop samples are also prone to weathering,

which can severely alter the organic composition (Clayton and Swetland, 1978). It is therefore crucial to assess these factors given the nature of the samples in this study.

Aromatic HCs may constitute 25–60% of oils derived from marine organic matter, but only around 10–30% of oils from non-marine organic matter (Tissot and Welte, 1984). The Botneheia Fm. ranges from kerogen type III/II in the lower Muen Mb. F1 mudstones to dominantly kerogen type II in the middle Blanknuten Mb. F3 mudstones (Krajewski, 2013). These two sub-units show the largest contrast in kerogen type (Fig. 3) and richness (Fig. 9), implying that they should also record a strong contrast in SAT/ARO ratios. Indeed, this is consistent for both the Blanknuten and Skrukkefjellet localities in this study (Figs. 14 and 15), suggesting that the source facies variations are the most important influences on the relative bitumen composition in the studied sections.

The R_o data from this study and T_{max} data from Krajewski (2013) (Fig. 9) suggest that no significant maturity contrast exists within each sample profile (Fig. 9). This is consistent with Haile et al. (2018), who concluded that the thermal maturity of the Blanknuten and Skrukkefjellet localities constrains the regional burial history without any obvious influence from nearby sill intrusions. Both of the sampled sections are less than 100 m (Fig. 9), and a difference greater than c. 4 °C from bottom to top appears unreasonable based on previously determined geothermal gradients in the region, i.e. c. 40 °C/km (Braathen et al., 2012). Thus, differential thermal maturation is considered a minor or insignificant influence on the relative bitumen content or composition throughout the study localities.

Previously published gas chromatography (FID) data of the Botneheia Fm. shales in the Blanknuten locality suggests incipient to mild biodegradation (Abay et al., 2014), indicating that biodegradation is unlikely to have caused major compositional changes to the studied bitumen in both localities.

Forsberg and Bjorøy (1983) found that the total EOM content in weathered shales from the Botneheia Fm. was reduced by an average of 10% compared to non-weathered shales from shallow, meter-deep boreholes. In addition, SAT/ARO ratios were generally higher in the cores than in the outcrop samples (up to 54% greater), showing a preferential loss of aromatic HCs vs. saturated HCs in weathered vs. "non-weathered" shale. These losses are considerably less than the variations observed in this study (Figs. 13 and 15).

From the discussion above, we interpret the kerogen richness and quality to be the dominating factors that influence the SAT/ARO ratio and the absolute and relative bulk bitumen fractions. However, we cannot rule out the possibility that minor influences of thermal maturation, weathering and biodegradation affect the facies differentially throughout the formation.

5.5. Relating bitumen content to source rock quality and richness

Studies of thin-sections (Krajewski, 2013) show that the lower–middle Muen Mb. F1 mudstones contain mostly marine macerals (lamalignite and telalginite) but elevated content of terrestrial macerals (vitrodetrinite, collinite, hebamorphinite and inertodetrinite). In contrast, the middle Blanknuten Mb. F3 mudstones contain dominantly amorphous organic matter, lamalginite and telalginite that show low degree of reworking and only negligible amounts of vitrinite (mostly telinite and vitrodetrinite) (Krajewski, 2013). These stratigraphic units therefore reflect organic petrological end-members in the Botneheia Fm. in terms of organic matter type. The upper Muen Mb. (F2) and the lower and upper Blanknuten Mb. (F2 and F4) show an intermediate composition (Krajewski, 2013). The SAT/ARO ratios are highest in the lower–middle Muen Mb. F1 mudstones (median 5.56), and lowest in the middle Blanknuten Mb. F3 mudstones (median 0.70), with the remaining stratigraphic units generally showing intermediate values (Fig. 15). It therefore appears that the total EOM (Fig. 13) and the SAT/ARO trends (Fig. 15) directly reflect the inferred relative content of terrestrial vs. marine maceral types throughout the Botneheia Fm. The highstand conditions and the resulting Early Ladinian maximum flooding surface appear to have favored abundant preservation and accumulation of marine organic matter, in accordance with Krajewski and Weitschat (2015).

The bitumen and TOC content of immature shales typically indicates their petroleum generation potential: the higher, the better (Peters and Cassa, 1994). EOM may correlate strongly with the S_1 parameter from Rock-Eval pyrolysis (Bhullar et al., 2000; Othman, 2004), since both parameters quantify free hydrocarbons within the mudstones. The relative EOM vs. TOC distribution of all the stratigraphic units in the Botneheia Fm. (Fig. 16) is consistent with the reported maceral composition and source rock richness and quality as determined by Rock-Eval (Krajewski, 2013). Still, it appears that the EOM vs. TOC plot overestimates the source potential for the Tschermakfjellet Fm. F1 mudstones as this formation is considered gas-prone only (Abay et al., 2018; Krajewski, 2013; Mueller et al., 2014; Mørk and Bjorøy, 1984). However, Krajewski (2013) describes the lowermost Tschermakfjellet Fm. samples as black shales and reports two immature samples with TOC values of 1.99 and 1.61 wt. % and HI values of 201 and 195 mg HC/g TOC respectively, indicating borderline oil potential. Some liquid petroleum might therefore have been generated (but not expelled) in the lowermost few meters of the Tschermakfjellet Fm. in the Blanknuten locality, although this is speculative and would not amount to any significant HC volumes.

EOM/TOC ratios of all samples from the Skrukkefjellet (0.07–0.29, median 0.19) and Blanknuten (0.07–0.27, median 0.19) localities indicate that the Botneheia Fm. has generated petroleum in both localities (Peters and Cassa, 1994), in agreement with T_{max} and biomarker parameters from Schou et al. (1984). Bitumen in Botneheia Fm. mudstones from the Blanknuten locality is *in situ* (Abay et al., 2017), and is probably the same in the Skrukkefjellet locality. There is clear evidence of hydrocarbon generation and primary migration in the Blanknuten Mb. in the Blanknuten locality by the intriguing discovery of a late Anisian–Ladinian ammonoid (*Aristoptychites trochleaeformis*) with oil-filled, hollow chambers (Smelror and Sollid, 2007; Thieβen et al., 2019). This evidently illustrates that the Blanknuten Mb. has sufficient source rock quality and richness for primary migrated oil to occur. While such a discovery is inherently rare and has not been encountered in the Skrukkefjellet locality, the similar EOM/TOC ratios compared to the Blanknuten locality (Fig. 15) could be a result of generated petroleum that is retained within the mudstone facies.

5.6. Towards a chemostratigraphic framework through multivariate analysis

The lithology and geochemistry of sediments are genetically related to the depositional environment. Therefore, multivariate analysis of facies-dependent inorganic and/or organic geochemical parameters by principal component analysis (PCA) and hierarchical cluster analysis (HCA) are useful tools in identifying properties (or groups of properties) reflecting depositional environment of lithified sediments, rock extracts, or oils (Garcia et al., 2020; Lerch et al., 2017; Yurchenko et al., 2018). Such chemostratigraphic analyses are typically done using biomarker parameters that are resistant to e.g. thermal maturation and biodegradation (Peters et al., 2007). The presented chemostratigraphic and multivariate analyses in this study therefore differs in the way that it tests whether the qualitative and macroscopically identified mudstone facies F1–F4 can be distinguished based solely on their bulk geochemical assemblages or not.

The chemostratigraphic correlation between the lower–middle Muen Mb. F1 mudstones and the two F1 mudstones from the lower Tschermakfjellet Fm. (Fig. 18, cluster C3) justifies the grouping of these two units into a common facies F1. This supports a similar depositional environment for these samples. Oxygenated conditions are known to preferentially preserve less labile terrestrial organic matter compared to

marine, lipid-rich organic matter (Demaison and Moore, 1980), which could have resulted in the high SAT/ARO ratios. Another explanation could be an overall elevated supply of terrestrial organic matter relative to the other facies types (i.e. F2, F3 or F4).

The single F1 sample in cluster C1 deviates significantly from the other F1 samples mudstones from the Tschermakfjellet Fm. and the lower–middle Muen Mb. (Fig. 18). Similar to the Blanknuten locality, Riis et al. (2008) report dark shales in the lowermost Carnian succession on the shelf east of Edgeøya. These lowermost Carnian shales show upwards decreasing source quality and richness (Xu et al., 2014), likely related to the upwards grading into the deltaic sandstones of the De Geerdalen Fm&tnqh_x02025 The base part of the Tschermakfjellet Fm. in eastern Svalbard and the shelf east of Edgeøya might reflect gradually less reworked upper Botneheia Fm. sediments or continuous sedimentation across the Ladinian–Carnian boundary. The latter was proposed by Høy and Lundschien (2011) to occur in the offshore Northern Norwegian Barents Sea. The Tschermakfjellet Fm. F1 sample of cluster C1 (Fig. 18) might therefore represent a more ventilated and proximal facies that better represents the entire Tschermakfjellet Fm.

The F2 mudstones from the upper Muen Mb. and the lower and upper Blanknuten Mb. are split between the clusters C2 and C4, indicating that the geochemical assemblages of these samples vary considerably (Figs. 17 and 18). However, the matching between the F2 mudstones from the upper Muen Mb. and the lower Blanknuten Mb. indicates that they were deposited during the same late transgressive phase, and that they therefore are genetically related (Krajewski, 2013). Macroscopic allochthonous phosphate nodule layers (Fig. 7a) shows that the F2 mudstones were deposited during hydrodynamically active bottom conditions, and varying compositional variations of these F2 mudstones should be expected (Krajewski, 2008). The correlation with absolute SAT and normalized SAT (%) for the dominant part of the F2 mudstones (Fig. 17) might indicate fairly well-preserved terrestrial organic matter that was provided before and after the deposition of F3 mudstones, which on the other hand show very low contributions of terrestrial organic matter (Krajewski, 2013).

The massive and well-laminated middle Blanknuten Mb. F3 mudstones and their strongly positive PC1 scores (Fig. 17) reflect the greatest absolute bitumen content and TOC among the analyzed facies (Table 2). These geochemical properties demarcate a distinct F3 mudstone group from the remaining sample set (Fig. 17) and provide overall good chemostratigraphic criteria to distinguish this facies. Still, it is evident that geochemical overlap between F2, F3 and F4 takes place as shown in cluster C2 and C4 (Fig. 18). This could be due to episodes of weak oxygenation and hydrodynamic reworking that caused source rock heterogeneity within the F3 mudstones (Krajewski, 2013). However, the organic matter composition is dominantly marine and highly oil prone (Krajewski, 2013), resulting in the specific distribution of normalized bulk bitumen fractions and very low SAT/ARO ratios that are unique for the F3 mudstones (Figs. 14 and 17; Table 2).

Four out of six F4 mudstone samples form a recognizable group based on the PCA (Fig. 17), correlating to the cluster C5 in the HCA (Fig. 18). This distinction from the lower and middle Blanknuten Mb. indicates a change in depositional environment that corresponds to the onset of a regressive phase with increased content of terrestrial organic matter and TIC from bivalve shell fragments (Krajewski, 2013; Mørk and Bromley, 2008). Currently we have no explanation for the elevated normalized polar fraction of the F4 mudstones (Fig. 17), but it may be due to increased sulfurization of saturated and unsaturated hydrocarbons (Tissot and Welte, 1984), which is more common in carbonates compared to siliciclastic mudstones (Jones, 1984). Although not specified in detail, Høy and Lundschien (2011) noted an abrupt change in the chemical conditions in this part of the Botneheia Fm., which could be partly captured by the HCA as cluster C5 (Fig. 18). The TIC content (Figs. 9 and 18) and normalized polar fraction (Figs. 14 and 17) provide the best bulk parameters to distinguish the regressive, calcareous F4 mudstones from F2 and F3 in the lower and middle Blanknuten Mb. respectively.

From the analysis above, the non-phosphogenic (lower–middle Muen Mb.) F1 mudstones and the phosphogenic (upper Muen Mb. to upper Blanknuten Mb.) F2–F4 mudstones are clearly distinguished without detailed analyses of the phosphate content or microfacies descriptions. This is important, because these two successions form principally different source rocks of dominantly kerogen type III/II and II respectively (Krajewski, 2013). In cases with highly fragmented sample material, e.g. when analyzing drill cuttings, textural and structural facies descriptions of mudstones are challenging. The coupling between facies and multivariate analysis may contribute to a lithostratigraphic and chemostratigraphic framework with use in the regional northern Norwegian Barents Shelf.

6. Conclusions

The Middle Triassic Botneheia Fm. in Svalbard represents the onshore counterpart to potentially important regional oil-prone source rocks in the Norwegian part of the Barents Shelf. Despite being one of the most attractive play models, the many disappointing exploration campaigns demonstrate that the Triassic petroleum system is not fully understood. The presence, distribution, richness and quality of the Lower–Middle Triassic organic-rich shales are among the risk factors. Because of the limited amount of core data available for detailed geochemical studies, outcrop investigations of analogue source rock units onshore Svalbard are very important for gaining a comprehensive understanding of their facies development on the Barents Shelf.

The presented investigation of organic-rich mudstone facies of the Botneheia Fm. in eastern Svalbard coupled with high-resolution chemostratigraphy sheds new light on the stratigraphic distribution of TS, TOC, TIC and bulk bitumen content in relation to the changing paleodepositional environments and benthic oxygen conditions. The mudstone facies-transitions forth and back from dark gray (F1) to black (F2 or F4), bioturbated mudstones via black, paper-laminated shale (F3) appears to be closely tied to the relative and absolute abundance of terrestrial vs. marine organic matter. This ratio, as inferred from the TOC and bulk bitumen content, is at a maximum in the Anisian and Carnian F1 mudstones, intermediate in the upper Anisian F2 and upper Ladinian F2 and F4 mudstones, and minimum in the lower Ladinian F3 mudstones. The high marine organic matter content in the F3 mudstones was probably a result of deeper, upwelled and nutrient rich waters that promoted high primary productivity in the photic zone which was subsequently exported to the sediment surface during early Ladinian time. The deposited necromass caused extensive phosphate precipitation within the mudstone matrix and concurrently the development of bottom water oxygen deficiency and TS enrichment. This resulted in less efficient organic matter degradation and therefore preservation of oil-prone kerogen. At this time, terrestrial organic matter and detrital input were at a minimum. The documented facies and chemostratigraphic trends, where the early Ladinian marks a defining turning point, may thus reflect the development of a pan-Arctic Middle Triassic transgressive–regressive sequence identified by previous studies.

This study shows that the non-phosphogenic lower–middle Muen Mb. differs substantially in facies and geochemistry from the phosphogenic mudstones of the upper Muen Mb. and the Blanknuten Mb. The former succession was likely deposited in a ventilated and oxygenated pro-deltaic to open shelf environment, while the latter succession was deposited in a deeper, more restricted dysoxic/anoxic shelf setting. The lack of high productivity and the low preservation potential in the non-phosphogenic lower–middle Muen Mb. are the main factors that promote the clear difference in TOC and bitumen content compared to the phosphogenic upper Muen and entire Blanknuten mbs. The suggested chemostratigraphic approach combined with the mudstone facies analysis could therefore be applied during exploration campaigns when only sidewall cores or cuttings are available to identify these principally different non-phosphogenic and phosphogenic source rock units

respectively.

The exploratory data analyses presented in this study partly distinguish the genetic differences between mudstones that may reflect separable sequence stratigraphic phases within the Middle Triassic Botneheia Fm. We therefore consider the exploratory data analysis as an applicable approach to link the geochemical content and the facies development of the Botneheia Fm. However, it is evident that the presented bulk geochemistry of the phosphogenic F2, F3, and F4 mudstones and their associated lithostratigraphic subunits within this formation overlap, and that the chemostratigraphic framework lacks sufficient resolution to clearly separate these units or facies.

7. Computer code availability

- Name of code: Wesenlund_et_al_2021_MPG.py
- Developer: Fredrik Wesenlund
- Contact details: Fredrik Wesenlund, Department of Geosciences, UiT–The Arctic University of Norway, Tromsø, Norway; email: Fredrik.wesenlund@uit.no; Year first available: 2021
- Hardware used: The Python script was developed and run on a notebook PC with a quad core CPU @ 1.60–2.11 GHz and 16 GB RAM
- Software used and required: The Python script was developed with the Anaconda 2020.11 Python distribution platform using Spyder 4.1.5 and needs the pandas, matplotlib, seaborn, scikit-learn, numpy and plotly (including express and orca) packages
- Program language: the code is written in Python 3.8.5
- Total size of script: c. 30 KB
- Details on how to access the source code: the source file can be downloaded from GitHub: https://github.com/fredrwes/Publications.

Declaration of competing interest

The authors declare that they have no known competing financial interests or personal relationships that could have appeared to influence the work reported in this paper.

Acknowledgments

This study forms part of the ARCEx consortium (Research Centre for Arctic Petroleum Exploration) which is funded by the Research Council of Norway (grant number 228107) and ARCEx partners. We are grateful for additional economic support from Lundin Energy Norway and the Norwegian Petroleum Directorate for the field expedition to Edgeøya. Atle Mørk is thanked for field expedition planning, logistics and great companionship, and the crew at research vessel SS Youexplore by The Dale Oen Experience for safe execution. Sofie Bernhardsen is acknowledged for field assistance and scientific contributions. Trine Dahl, Ingvild Hald and Karina Monsen are thanked for help and discussions in the geology lab at UiT–The Arctic University of Norway. Kristian Backer-Owe and Dag Arild Karlsen are appreciated for permission to use the organic geochemical lab at the University of Oslo, and the Petroleum Research School of Norway (NFiP) are thanked for covering travel expenses. Comments and suggestions by Associate Editor Richard Patience and the anonymous reviewers that helped to improve the manuscript are gratefully acknowledged.

Appendix A. Supplementary data

Supplementary data to this article can be found online at https://doi.org/10.1016/j.marpetgeo.2021.105168.

Credit author statement

Fredrik Wesenlund: Conceptualization, Methodology, Software, Validation, Formal analysis, Investigation, Data Curation, Writing – original draft, Visualization. Sten-Andreas Grundvåg: Investigation, Writing - Review & Editing, Supervision, Project administration, Funding acquisition. Victoria Sjøholt Engelschiøn: Investigation, Data Curation, Validation, Writing - Review & Editing. Olaf Thieβen: Conceptualization, Writing - Review & Editing, Supervision. Jon Halvard Pedersen: Conceptualization, Writing - Review & Editing, Supervision.

References

Abay, T.B., Karlsen, D.A., Pedersen, J.H., 2014. Source rocks at Svalbard: an overview of Jurassic and Triassic formations and comparison with offshore Barents Sea time equivalent source rock formations. AAPG Datapages Search and Discovery, 30372. https://www.searchanddiscovery.com/documents/2014/30372abay/ndx_abay.pdf.

Abay, T.B., Karlsen, D.A., Lerch, B., Olaussen, S., Pedersen, J.H., Backer-Owe, K., 2017. Migrated petroleum in outcropping Mesozoic sedimentary rocks in Spitsbergen: organic geochemical characterization and implications for regional exploration. J. Petrol. Geol. 40, 5–36.

Abay, T.B., Karlsen, D.A., Pedersen, J.H., Olaussen, S., Backer-Owe, K., 2018. Thermal maturity, hydrocarbon potential and kerogen type of some Triassic–Lower Cretaceous sediments from the SW Barents Sea and Svalbard. Petrol. Geosci. 24, 349–373.

Abdullah, W.H., 1999. Organic facies variations in the Triassic shallow marine and deep marine shales of central Spitsbergen, Svalbard. Mar. Petrol. Geol. 16, 467–481.

Alsen, P., McRoberts, C., Svennevig, K., Bojesen-Koefoed, J., Hovikoski, J., Piasecki, S., 2017. The Israd Formation: a Middle Triassic Daonella-bearing, black shale unit in Kilen, North Greenland (with a note on the Triassic in Amdrup Land). Newsl. Stratigr. 50, 31–46.

Alsenz, H., Illner, P., Ashckenazi-Polivoda, S., Meilijson, A., Abramovich, S., Feinstein, S., Almogi-Labin, A., Berner, Z., Püttmann, W., 2015. Geochemical evidence for the link between sulfate reduction, sulfide oxidation and phosphate accumulation in a Late Cretaceous upwelling system. Geochem. Trans. 16, 13.

Anell, I., Braathen, A., Olaussen, S., Osmundsen, P.T., 2013. Evidence of faulting contradicts a quiescent northern Barents Shelf during the Triassic. First Break 31, 67–76.

Anell, I., Zuchuat, V., Röhnert, A.D., Smyrak-Sikora, A., Buckley, S., Lord, G., Maher, H., Midtkandal, I., Ogata, K., Olaussen, S., Osmundsen, P.T., Braathen, A., 2020. Tidal amplification and along-strike process variability in a mixed-energy paralic system prograding onto a low accommodation shelf, Edgeøya, Svalbard. Basin Res. 33, 478–512.

Arthur, M.A., Sageman, B.B., 1994. Marine black shales - depositional mechanisms and environments of ancient deposits. Annu. Rev. Earth Planet Sci. 22, 499–551.

Berner, R.A., Raiswell, R., 1983. Burial of organic-carbon and pyrite sulfur in sediments over phanerozoic time - a new theory. Geochem. Cosmochim. Acta 47, 855–862.

Bernhardsen, S., 2019. A sedimentological study of the organic-rich Botneheia Formation (Middle Triassic) with emphasis on the ichnogenus Thalassinoides, Edgeøya, Svalbard. MSc thesis. Norwegian University of Science and Technology (NTNU), Trondheim, Norway, p. 142.

Bhullar, A.G., Karlsen, D.A., Backer-Owe, K., Le Tran, K., Skalnes, E., Berchelmann, H.H., Kittelsen, J.E., 2000. Reservoir characterization by a combined micro-extraction - micro thin-layer chromatography (Iatroscan) method: a calibration study with examples from the Norwegian North Sea. J. Petrol. Geol. 23, 221–244.

Bjerager, M., Alsen, P., Hovikoski, J., Lindstrom, S., Pilgaard, A., Stemmerik, L., Therkelsen, J., 2019. Triassic lithostratigraphy of the Wandel Sea Basin, North Greenland. Bull. Geol. Soc. Den. 67, 83–105.

Bjorøy, M., Hall, P.B., Ferriday, I.L., Mørk, A., 2009. Triassic Source Rocks of the Barents Sea and Svalbard. AAPG Datapages Search and Discovery, 10219. https://www.searchanddiscovery.com/documents/2009/10219bjoroy/ndx_bjoroy.pdf.

Brekke, T., Krajewski, K.P., Hubred, J.H., 2014. Organic geochemistry and petrography of thermally altered sections of the Middle Triassic Botneheia Formation on southwestern Edgeøya, Svalbard. Norwegian Petroleum Directorate Bulletin 11, 111–128.

Bromley, R.G., Ekdale, A.A., 1984. *Chondrites*: a trace fossil indicator of anoxia in sediments. Science 224, 872–874.

Braathen, A., Baelum, K., Christiansen, H.H., Dahl, T., Eiken, O., Elvebakk, H., Hansen, F., Hanssen, T.H., Jochmann, M., Johansen, T.A., Johnsen, H., Larsen, L., Lie, T., Mertes, J., Mørk, A., Mørk, M.B., Nemec, W., Olaussen, S., Oye, V., Rod, K., Titlestad, G.O., Tveranger, J., Vagle, K., 2012. The Longyearbyen CO2 Lab of Svalbard, Norway-initial assessment of the geological conditions for CO2 sequestration. Norw. J. Geol. 92, 353–376.

Buckley, S.J., Ringdal, K., Naumann, N., Dolva, B., Kurz, T.H., Howell, J.A., Dewez, T.J. B., 2019. LIME: software for 3-D visualization, interpretation, and communication of virtual geoscience models. Geosphere 15, 222–235.

Byers, C.W., 1974. Shale fissility - relation to bioturbation. Sedimentology 21, 479–484.

Clayton, J.L., Swetland, P.J., 1978. Subaerial weathering of sedimentary organic-matter. Geochem. Cosmochim. Acta 42, 305–312.

Creaney, S., Passey, Q.R., 1993. Recurring patterns of total organic carbon and source rock quality within a sequence stratigraphic framework. AAPG (Am. Assoc. Pet. Geol.) Bull. 77, 386–401.

Dallmann, W.K., Elvevold, S., 2015. Bedrock geology. In: Dallmann, W. (Ed.), Geoscience Atlas of Svalbard. Norwegian Polar Institute.

Demaison, G.J., Moore, G.T., 1980. Anoxic environments and oil source bed genesis. AAPG (Am. Assoc. Pet. Geol.) Bull. 64, 1179–1209.

Demaison, G.J., Huizinga, B.J., 1991. Genetic classification of petroleum systems. AAPG (Am. Assoc. Pet. Geol.) Bull. 75, 1626–1643.
Dembicki, J.H., 2009. Three common source rock evaluation errors made by geologists during prospect or play appraisals. AAPG (Am. Assoc. Pet. Geol.) Bull. 93, 341–356.
Dembicki, J.H., 2017. Source rock evaluation. In: Dembicki, J.H. (Ed.), Practical Petroleum Geochemistry for Exploration and Production. Elsevier, pp. 61–133.
England, W.A., Mackenzie, A.S., 1989. Some aspects of the organic geochemistry of petroleum fluids. Geol. Rundsch. 78, 291–303.
Faleide, J.I., Gudlaugsson, S.T., Jacquart, G., 1984. Evolution of the western Barents Sea. Mar. Petrol. Geol. 1, 123–150.
Faleide, J.I., Bjørlykke, K., Gabrielsen, R.H., 2015. Geology of the Norwegian continental shelf. In: Bjørlykke, K. (Ed.), Petroleum Geoscience: from Sedimentary Environments to Rock Physics. Springer Berlin Heidelberg, Berlin, Heidelberg, pp. 603–637.
Filippelli, G.M., 2011. Phosphate rock formation and marine phosphorus geochemistry: the deep time perspective. Chemosphere 84, 759–766.
Forsberg, A., Bjorøy, M., 1983. A sedimentological and organic geochemical study of the Botneheia Formation, Svalbard, with special emphasis on the effects of weathering on the organic matter in shales. In: Bjorøy, M., Albrecht, P., Cornford, C., others (Eds.), Advances in Organic Geochemistry 1981. Wiley, Chichester, pp. 60–68.
Garcia, R.J.L., da Silva, J.B., Abreu, I.M., Soares, S.A.R., Araujo, R.G.O., de Souza, E.S., Ribeiro, H.J.S., Hadlich, G.M., Queiroz, A.F.D., 2020. Application of PCA and HCA in geochemical parameters to distinguish depositional paleoenvironments from source rocks. J. S. Am. Earth Sci. 103.
Ghadeer, S.G., Macquaker, J.H.S., 2012. The role of event beds in the preservation of organic carbon in fine-grained sediments: analyses of the sedimentological processes operating during deposition of the Whitby Mudstone Formation (Toarcian, Lower Jurassic) preserved in northeast England. Mar. Petrol. Geol. 35, 309–320.
Ghassal, B.I., Littke, R., El Atfy, H., Sindern, S., Scholtysik, G., El Beialy, S., El Khoriby, E., 2018. Source rock potential and depositional environment of Upper Cretaceous sedimentary rocks, Abu Gharadig Basin, Western Desert, Egypt: an integrated palynological, organic and inorganic geochemical study. Int. J. Coal Geol. 186, 14–40.
Glørstad-Clark, E., Faleide, J.I., Lundschien, B.A., Nystuen, J.P., 2010. Triassic seismic sequence stratigraphy and paleogeography of the western Barents Sea area. Mar. Petrol. Geol. 27, 1448–1475.
Glørstad-Clark, E., Birkeland, E.P., Nystuen, J.P., Faleide, J.I., Midtkandal, I., 2011. Triassic platform-margin deltas in the western Barents Sea. Mar. Petrol. Geol. 28, 1294–1314.
Haile, B.G., Klausen, T.G., Jahren, J., Braathen, A., Hellevang, H., 2018. Thermal history of a Triassic sedimentary sequence verified by a multi-method approach: Edgeøya, Svalbard, Norway. Basin Res. 30, 1075–1097.
Haremo, P., Andresen, A., Dypvik, H., Nagy, J., Elverhøi, A., Eikeland, T.A., Johansen, H., 1990. Structural development along the Billefjorden Fault Zone in the area between Kjellströmdalen and Adventdalen/Sassendalen, central Spitsbergen. Polar Res. 8, 195–216.
Henriksen, E., Bjørnseth, H.M., Hals, T.K., Heide, T., Kiryukhina, T., Kløvjan, O.S., Larssen, G.B., Ryseth, A.E., Rønning, K., Sollid, K., Stoupakova, A., 2011. Uplift and erosion of the greater Barents Sea: impact on prospectivity and petroleum systems. In: Spencer, A.M., Embry, A.F., Gautier, D.L., Stoupakova, A.V., Sørensen, K. (Eds.), Arctic Petroleum Geology. The Geological Society of London, pp. 271–281.
Hounslow, M.W., Hu, M.Y., Mørk, A., Weitschat, W., Vigran, J.O., Karloukovski, V., Orchard, M.J., 2008. Intercalibration of Boreal and Tethyan time scales: the magnetobiostratigraphy of the Middle Triassic and the latest Early Triassic from Spitsbergen, Arctic Norway. Polar Res. 27, 469–490.
Hubred, J.H., 2006. Thermal effects of basaltic sill emplacement in source rocks on maturation and hydrocarbon generation. Department of Geosciences, University of Oslo, Oslo, Norway. Cand. Scient. thesis.
Høy, T., Lundschien, B.A., 2011. Triassic deltaic sequences in the northern Barents Sea. In: Spencer, A.M., Embry, A.F., Gautier, D.L., Stoupakova, A.V., Sørensen, K. (Eds.), Arctic Petroleum Geology. The Geological Society of London, pp. 249–260.
Ineson, J.R., Hovikoski, J., Sheldon, E., Piasecki, S., Alsen, P., Fyhn, M.B.W., Bjerager, M., Dybkjaer, K., Guarnieri, P., Lauridsen, B.W., Nohr-Hansen, H., Pedersen, G.K., Svennevig, K., Therkelsen, J., Weibel, R., Bojesen-Koefoed, J.A., 2021. Regional impact of Early Cretaceous tectono-magmatic uplift in the Arctic: implications of new data from eastern North Greenland, 33. Terra Nova, pp. 284–292.
Jones, R.W., 1984. Comparison of carbonate and shale source rocks. In: Palacas, J.G. (Ed.), Petroleum Geochemistry and Source Rock Potential of Carbonate Rocks. American Association of Petroleum Geologists.
Karlsen, D.A., Larter, S.R., 1991. Analysis of petroleum fractions by TLC-FID - applications to petroleum reservoir description. Org. Geochem. 17, 603–617.
Klausen, T.G., 2013. Does evidence of faulting contradict a quiescent northern Barents Shelf during the Triassic? First Break 31, 69–72.
Klausen, T.G., Ryseth, A.E., Helland-Hansen, W., Gawthorpe, R., Laursen, I., 2015. Regional development and sequence stratigraphy of the Middle to Late Triassic Snadd Formation, Norwegian Barents Sea. Mar. Petrol. Geol. 62, 102–122.
Klausen, T.G., Nyberg, B., Helland-Hansen, W., 2019. The largest delta plain in Earth's history. Geology 47, 470–474.
Krajewski, K.P., 2008. The Botneheia Formation (Middle Triassic) in Edgeøya and Barentsøya, Svalbard: lithostratigraphy, facies, phosphogenesis, paleoenvironment. Pol. Polar Res. 29, 319–364.
Krajewski, K.P., 2013. Organic matter–apatite–pyrite relationships in the Botneheia Formation (Middle Triassic) of eastern Svalbard: relevance to the formation of petroleum source rocks in the NW Barents Sea shelf. Mar. Petrol. Geol. 45, 69–105.
Krajewski, K.P., Weitschat, W., 2015. Depositional history of the youngest strata of the Sassendalen Group (Bravaisberget Formation, Middle Triassic–Carnian) in southern Spitsbergen, Svalbard. Ann. Soc. Geol. Pol. 85, 151–175.
Law, C.A., 1999. Evaluating source rocks. In: Beaumont, E.A., Foster, N.H. (Eds.), Exploring for Oil and Gas Traps, 1 ed. AAPG, pp. 1–41.
Le Tran, K., Philippe, B., 1993. Oil and rock extract analysis. In: Bordenave, M.L. (Ed.), Applied Petroleum Geochemistry. Editions Technip, pp. 376–394.
Leith, T.L., Weiss, H.M., Mørk, A., Århus, N., Elvebakk, G., Embry, A.F., Brooks, P.W., Stewart, K.R., Pchelina, T.M., Bro, E.G., Verba, M.L., Danyushevskaya, A., Borisov, A.V., 1992. Mesozoic hydrocarbon source rocks of the Arctic region. In: Vorren, T.O., Bergsager, E., Dahl-Stamnes, A., Holter, E., Johansen, Å., Lie, Å., Lund, T.B. (Eds.), Arctic Geology and Petroleum Potential. Elsevier, Amsterdam, pp. 1–25.
Lerch, B., Karlsen, D.A., Abay, T.B., Duggan, D., Seland, R., Backer-Owe, K., 2016. Regional petroleum alteration trends in Barents Sea oils and condensates as a clue to migration regimes and processes. AAPG (Am. Assoc. Pet. Geol.) Bull. 100, 165–190.
Lerch, B., Karlsen, D.A., Seland, R., Backer-Owe, K., 2017. Depositional environment and age determination of oils and condensates from the Barents Sea. Petrol. Geosci. 23, 190–209.
Lerch, B., Karlsen, D.A., Thiessen, O., Abay, T.B., van Soelen, E.E., Kurschner, W.M., Planke, S., Backer-Owe, K., 2018. Investigations on the use of triaromatic dimethylcholesteroids as age-specific biomarkers in bitumens and oils from Arctic Norway. Org. Geochem. 122, 1–16.
Leventhal, J.S., 1995. Carbon-sulfur plots to show diagenetic and epigenetic sulfidation in sediments. Geochem. Cosmochim. Acta 59, 1207–1211.
Lord, G.S., Johansen, S.K., Støen, S.J., Mørk, A., 2017. Facies development of the Upper Triassic succession on Barentsøya, Wilhelmøya and NE Spitsbergen, Svalbard. Norw. J. Geol. 97, 33–62.
Lundschien, B.A., Høy, T., Mørk, A., 2014. Triassic hydrocarbon potential in the Northern Barents Sea; integrating Svalbard and stratigraphic core data. Norwegian Petroleum Directorate Bulletin 11, 3–20.
MacEachern, J.A., Pemberton, S.G., Bann, K.L., Gingras, M.K., 2009. Departures from the archetypal ichnofacies: effective recognition of physico-chemical stresses in the rock record. In: MacEachern, J.A., Bann, K.L., Gingras, M.K., Pemberton, S.G. (Eds.), Applied Ichnology. SEPM Society for Sedimentary Geology, Tulsa, Oklahoma, USA, pp. 64–94.
Maher, H.D., Hays, T., Shuster, R., Mutrux, J., 2004. Petrography of Lower Cretaceous sandstones on Spitsbergen. Polar Res. 23, 147–165.
Marshall, C., Uguna, J., Large, D.J., Meredith, W., Jochmann, M., Friis, B., Vane, C., Spiro, B.F., Snape, C.E., Orheim, A., 2015. Geochemistry and petrology of Palaeocene coals from Spitzbergen — Part 2: Maturity variations and implications for local and regional burial models. Int. J. Coal Geol. 143, 1–10.
Marynowski, L., Kurkiewicz, S., Rakocinski, M., Simoneit, B.R.T., 2011. Effects of weathering on organic matter: I. Changes in molecular composition of extractable organic compounds caused by paleoweathering of a Lower Carboniferous (Tournaisian) marine black shale. Chem. Geol. 285, 144–156.
Matapour, Z., Karlsen, D.A., Lerch, B., Backer-Owe, K., 2019. Petroleum occurrences in the carbonate lithologies of the Gohta and Alta discoveries in the Barents Sea, Arctic Norway. Petrol. Geosci. 25, 50–70.
Morse, J.W., Emeis, K.C., 1990. Controls on C/S ratios in hemipelagic upwelling sediments. Am. J. Sci. 290, 1117–1135.
Mueller, S., Veld, H., Nagy, J., Kürschner, W.M., 2014. Depositional history of the Upper Triassic Kapp Toscana Group on Svalbard, Norway, inferred from palynofacies analysis and organic geochemistry. Sediment. Geol. 310, 16–29.
Muller, R., Klausen, T.G., Faleide, J.I., Olaussen, S., Eide, C.H., Suslova, A., 2019. Linking regional unconformities in the Barents Sea to compression-induced forebulge uplift at the Triassic-Jurassic transition. Tectonophysics 765, 35–51.
Mørk, A., Knarud, R., Worsley, D., 1982. Depositional and diagenetic environments of the Triassic and Lower Jurassic succession of Svalbard. In: Embry, A.F., Balkwill, H.R. (Eds.), Arctic Geology and Geophysics: Proceedings of the Third International Symposium on Arctic Geology, vol. 8. Canadian Society of Petroleum Geologists Memoir, pp. 371–398.
Mørk, A., Bjorøy, M., 1984. Mesozoic source rocks on Svalbard. In: Spencer, A.M. (Ed.), Proceedings of the North European Margin Symposium (NEMS '83), Organized by the Norwegian Petroleum Society and Held at the Norwegian Institute of Technology (NTH) in Trondheim 9–11 May. Springer Netherlands, pp. 371–382.
Mørk, A., Embry, A., Weitschat, W., 1989. Triassic transgressive-regressive cycles in the Sverdrup Basin, Svalbard and the Barents shelf. In: Collinson, J. (Ed.), Correlation in Hydrocarbon Exploration. Graham and Trotman, Bergen, Norway, pp. 113–130.
Mørk, A., Dallmann, W.K., Dypvik, H., Johannessen, E.P., Larssen, G.B., Nagy, J., Nøttvedt, A., Olaussen, S., Pčelina, T.M., Worsley, D., 1999. Mesozoic lithostratigraphy. In: Dallmann, W.K. (Ed.), Lithostratigraphic Lexicon of Svalbard. Norwegian Polar Institute, pp. 127–214.
Mørk, A., Elvebakk, G., 1999. Lithological description of subcropping Lower and Middle Triassic rocks from the Svalis Dome, Barents Sea. Polar Res. 18, 83–104.
Mørk, A., Bromley, R.G., 2008. Ichnology of a marine regressive systems tract: the Middle Triassic of Svalbard. Polar Res. 27, 339–359.
Mørk, A., 2015. Historical geology. In: Dallmann, W. (Ed.), Geoscience Atlas of Svalbard. Norwegian Polar Institute.
Norwegian Petroleum Directorate, 2017. Geological assessment of petroleum resources in eastern parts of Barents Sea north 2017. Norwegian Petroleum Directorate.
Norwegian Petroleum Directorate, 2020. Factpages. Norwegian Petroleum Directorate. http://factpages.npd.no/factpages/. (Accessed 20 November 2020).
Norwegian Polar Institute, 2020. Map view of Skrukkefjellet. Norwegian Polar Institute. https://toposvalbard.npolar.no/. (Accessed 20 November 2020).

Ogata, K., Mulrooney, M.J., Braathen, A., Maher, H., Osmundsen, P.T., Anell, I., Smyrak-Sikora, A.A., Balsamo, F., 2018. Architecture, deformation style and petrophysical properties of growth fault systems: the Late Triassic deltaic succession of southern Edgeøya (East Svalbard). Basin Res. 30, 1042–1073.

Ohm, S.E., Karlsen, D.A., Austin, T.J.F., 2008. Geochemically driven exploration models in uplifted areas: examples from the Norwegian Barents Sea. AAPG (Am. Assoc. Pet. Geol.) Bull. 92, 1191–1223.

Osmundsen, P.T., Braathen, A., Rød, R.S., Hynne, I.B., 2014. Styles of normal faulting and fault-controlled sedimentation in the Triassic deposits of Eastern Svalbard. Norwegian Petroleum Directorate Bulletin 11, 61–79.

Othman, R.S., 2004. Relationships between Rock-Eval S1 and extractable organic matter for selected source rock samples from New South Wales. 21th Annual Meeting of the Society for Organic Petrology, Sydney, New South Wales, Australia. https://archives.datapages.com/data/tsop/TSOPv21_2004/othman02.pdf.

Paterson, N.W., Mangerud, G., Mørk, A., 2017. Late Triassic (early Carnian) palynology of shallow stratigraphical core 7830/5-U-1, offshore Kong Karls Land. Norwegian Arctic. Palynology 41, 230–254.

Pedersen, T.F., Calvert, S.E., 1990. Anoxia vs productivity - what controls the formation of organic-carbon-rich sediments and sedimentary-rocks. AAPG (Am. Assoc. Pet. Geol.) Bull. 74, 454–466.

Peters, K.E., Cassa, M.R., 1994. Applied source rock geochemistry. In: Magoon, L.B., Dow, W.G. (Eds.), The Petroleum System - from Source to Trap. AAPG, pp. 93–120.

Peters, K.E., Walters, C.C., Moldowan, J.M., 2005. Biomarkers and Isotopes in Petroleum Systems and Earth History, the Biomarker Guide, 2 ed. Cambridge University Press.

Peters, K.E., Ramos, L.S., Zumberge, J.E., Valin, Z.C., Scotese, C.R., Gautier, D.L., 2007. Circum-Arctic petroleum systems identified using decision-tree chemometrics. AAPG (Am. Assoc. Pet. Geol.) Bull. 91, 877–913.

Potter, P.E., Maynard, J.B., Depetris, P.J., 2005. Mud and Mudstones. Springer-Verlag Berlin Heidelberg.

Redelius, P., Soenen, H., 2015. Relation between bitumen chemistry and performance. Fuel 140, 34–43.

Riis, F., Lundschien, B.A., Høy, T., Mørk, A., Mørk, M.B.E., 2008. Evolution of the Triassic shelf in the northern Barents Sea region. Polar Res. 27, 318–338.

Rodrigues Duran, E., di Primio, R., Anka, Z., Stoddart, D., Horsfield, B., 2013a. Petroleum system analysis of the Hammerfest Basin (southwestern Barents Sea): comparison of basin modelling and geochemical data. Org. Geochem. 63, 105–121.

Rodrigues Duran, E., di Primio, R., Anka, Z., Stoddart, D., Horsfield, B., 2013b. 3D-basin modelling of the Hammerfest Basin (southwestern Barents Sea): a quantitative assessment of petroleum generation, migration and leakage. Mar. Petrol. Geol. 45, 281–303.

Ruttenberg, K.C., Goni, M.A., 1997. Phosphorus distribution, C:N:P ratios, and $\delta^{13}C(oc)$ in arctic, temperate, and tropical coastal sediments: tools for characterizing bulk sedimentary organic matter. Mar. Geol. 139, 123–145.

Schatz, W., 2005. Palaeoecology of the Triassic black shale bivalve Daonella—new insights into an old controversy. Palaeogeogr. Palaeoclimatol. Palaeoecol. 216, 189–201.

Schieber, J., 2016. Mud re-distribution in epicontinental basins - exploring likely processes. Mar. Petrol. Geol. 71, 119–133.

Schou, L., Mørk, A., Bjorøy, M., 1984. Correlation of source rocks and migrated hydrocarbons by GC-MS in the Middle Triassic of Svalbard. Org. Geochem. 6, 513–520.

Senger, K., Tveranger, J., Ogata, K., Braathen, A., Planke, S., 2014. Late mesozoic magmatism in svalbard: a review. Earth Sci. Rev. 139, 123–144.

Smelror, M., Sollid, K., 2007. Blekkspruter fulle av olje. GEO 2, 28–29.

Smolarek, J., Marynowski, L., Trela, W., Kujawski, P., Simoneit, B.R.T., 2017. Redox conditions and marine microbial community changes during the end-Ordovician mass extinction event. Global Planet. Change 149, 105–122.

Smyrak-Sikora, A., Osmundsen, P.T., Braathen, A., Ogata, K., Anell, I., Mulrooney, M.J., Zuchuat, V., 2019. Architecture of growth basins in a tidally influenced, prodelta to delta-front setting: the Triassic succession of Kvalpynten, East Svalbard. Basin Res. 32, 949–978.

Stueland, E., 2016. Wisting – shallow reservoir. Possibilities and challenges. FORCE Underexplored Plays II, Stavanger, Norway. https://www.npd.no/globalassets/2-force/2019/documents/archive-2010-2018/underexplored-plays–part-ii/wisting—force-edited_underexplored-plays-ii-omv_v2_eirikstueland.pdf.

Thießen, O., Weiss, H.M., Smelror, M., Sollid, K., 2019. Triassic oil from the Botneheia Formation of Svalbard and oil-oil Correlation with recent Norwegian Barents Sea discoveries, 29th International Meeting on Organic Geochemistry. European Association of Organic Geochemists, Gothenburg, Sweden.

Tissot, B.P., Welte, D.H., 1984. Geological Control of Petroleum Type, Petroleum Formation and Occurrence, 2 ed. Springer-Verlag, Berlin, Germany, p. 699.

Traykovski, P., Geyer, W.R., Irish, J.D., Lynch, J.F., 2000. The role of wave-induced density-driven fluid mud flows for cross-shelf transport on the Eel River continental shelf. Continent. Shelf Res. 20, 2113–2140.

Vigran, J.O., Mangerud, G., Mørk, A., Bugge, T., Weitschat, W., 1998. Biostratigraphy and sequence stratigraphy of the Lower and Middle Triassic deposits from the Svalis Dome, central Barents Sea, Norway. Palynology 22, 89–141.

Vigran, J.O., Mørk, A., Forsberg, A.W., Weiss, H.M., Weitschat, W., 2008. Tasmanites algae—contributors to the Middle Triassic hydrocarbon source rocks of Svalbard and the Barents shelf. Polar Res. 27, 360–371.

Vigran, J.O., Mangerud, G., Mørk, A., Worsley, D., Hochuli, P.A., 2014. Palynology and geology of the Triassic succession of Svalbard and the Barents Sea. Geological Survey of Norway Special Publication 14.

Vossler, S.M., Pemberton, S.G., 1988. *Skolithos* in the Upper Cretaceous Cardium Formation: an ichnofossil example of opportunistic ecology. Lethaia 21, 351–362.

Wang, Y.-P., Zou, Y.-R., Shi, J.-T., Shi, J., 2018. Review of the chemometrics application in oil-oil and oil-source rock correlations. Journal of Natural Gas Geoscience 3, 217–232.

Waples, D.W., Curiale, J.A., 1999. Oil–oil and oil–source rock correlations. In: Beaumont, E.A., Foster, N.H. (Eds.), Exploring for Oil and Gas Traps. AAPG.

Weiss, H.M., Wilhelms, A., Mills, N., Scotchmer, J., Hall, P.B., Lind, K., Brekke, T., 2000. NIGOGA - The Norwegian Industry Guide to Organic Geochemical Analyses, 4th. Norsk Hydro, Statoil, Geolab Nor, SINTEF Petroleum Research and the Norwegian Petroleum Directorate.

Whittaker, A., Morton-Thompson, D., 1992. Mudlogging: drill cuttings analysis. In: Morton-Thompson, D., Woods, A.M. (Eds.), Development Geology Reference Manual. AAPG, Tulsa, Oklahoma, USA, pp. 104–105.

Wignall, P.B., 1991. Dysaerobic trace fossils and ichnofabrics in the Upper Jurassic Kimmeridge Clay of southern England. Palaios 6, 264–270.

Wilson, R.D., Schieber, J., 2014. Muddy prodeltaic hyperpycnites in the Lower Genesee Group of central New York, USA: implications for mud transport in epicontinental seas. J. Sediment. Res. 84, 866–874.

Wong, B., 2011. Color blindness. Nat. Methods 8, 441.

Xu, G.P., Hannah, J.L., Bingen, B., Georgiev, S., Stein, H.J., 2012. Digestion methods for trace element measurements in shales: paleoredox proxies examined. Chem. Geol. 324, 132–147.

Xu, G., Hannah, J.L., Stein, H.J., Mørk, A., Vigran, J.O., Bingen, B., Schutt, D.L., Lundschien, B.A., 2014. Cause of Upper Triassic climate crisis revealed by Re–Os geochemistry of Boreal black shales. Palaeogeogr. Palaeoclimatol. Palaeoecol. 395, 222–232.

Yurchenko, I.A., Moldowan, J.M., Peters, K.E., Magoon, L.B., Graham, S.A., 2018. The role of calcareous and shaly source rocks in the composition of petroleum expelled from the Triassic Shublik Formation, Alaska North Slope. Org. Geochem. 122, 52–67.